Remote Sensing of Environment 184 (2016) 58–72

Contents lists available at ScienceDirect

Remote Sensing of Environment

journal homepage: www.elsevier.com/locate/rse

Assessing hydro-ecological vulnerability using microwave radiometric measurements from WindSat

Dimitrios Stampoulis [a,*], Konstantinos M. Andreadis [a], Stephanie L. Granger [a], Joshua B. Fisher [a], Francis J. Turk [a], Ali Behrangi [a], Amor V. Ines [b], Narendra N. Das [a]

[a] Jet Propulsion Laboratory, California Institute of Technology, Pasadena, CA, USA
[b] Department of Biosystems and Agricultural Engineering, Michigan State University, East Lansing, MI, USA

ARTICLE INFO

Article history:
Received 25 November 2014
Received in revised form 28 May 2016
Accepted 5 June 2016
Available online xxxx

ABSTRACT

The spatial distribution, magnitude and timing of precipitation events are being altered globally, often leading to extreme hydrologic conditions with serious implications to the environment and society. Motivated by the pressing need to understand, from a hydro-ecological perspective, the impact of the dynamic nature of the hydrologic cycle on the environment in water-stressed regions, we investigated how different habitats in East Africa behave under extreme hydrologic conditions. We assessed the hydro-ecological vulnerability of the region by studying the response of soil moisture and vegetation water content to precipitation deficiency. The spatial patterns and characteristics of the inter-relations among the three aforementioned hydrologic variables, as well as the sensitivity and resilience of vegetation water content and soil moisture, derived from WindSat, were investigated for different vegetation types during dry spells of varying duration, identified using the Tropical Rainfall Measuring Mission (TRMM), in 2003–2011. Forest/Woody Savanna (FWS) and Savanna/Grasslands (SG) are more sensitive to local hydrologic extremes, while Shrublands (SHR) and the soils that support it are the least impacted by these conditions. SG and FWS exhibit the highest vegetation water content resilience, whereas soil moisture persistence during dry spells is at its highest in SHR/SG. The environmental variability, illustrated by the spatial patterns of the aforementioned hydrologic properties, can potentially play a role in the enhancement of resilience. This study provides critical insight into the hydro-ecological vulnerability of East Africa using microwave remote sensing, and this information can be used towards advancing management and decision support systems that would improve societal well-being and economic development.

1. Introduction

Water is the key environmental parameter that provides an interconnectedness among ecosystem components. Varying precipitation (P) patterns, vegetation, and soil moisture (SM) dynamics, are the linkages in a natural environment that determine the complexity in such systems (Asbjornsen et al., 2011; Dunbar & Acreman, 2001; Porporato & Rodriguez-Iturbe, 2002). In regions where water is constantly or seasonally limited, its spatial and temporal distribution determines the phenology and sustainability of vegetation regimes (McVicar, Roderick, Donohue, & Van Niel, 2012), and thus, influences the regional hydro-climatology and biotic composition (Wolff et al., 2011; D'Odorico & Bhattachan, 2012; Grimm et al., 2013; Fisher & Andreadis, 2014). Deviations from the average hydrologic patterns at the regional scale are generally not rare, often leading to floods or droughts. However, due to their dynamic nature, ecosystems are capable of adapting to different hydrologic conditions (Pickett, 1985; Sousa, 1984), as well as to short-term (Andela, Liu, van Dijk, de Jeu, & McVicar, 2013) and long-term (Donohue, Roderick, McVicar, & Farquhar, 2013) changes in other environmental resources. The interaction between the stress caused by extreme hydrologic conditions and an ecosystem's inherent capacity to respond determines the vulnerability of the ecosystem, which depends on its physiography, as well as the magnitude and duration of the stressor (Römer et al., 2012; Smith et al., 2014; Turner et al., 2003). Investigating the sensitivity of ecosystems to changes in P patterns, and their persistence in maintaining their stability offers a unique opportunity to better understand the mechanisms and interactions among ecosystem components, which is an intriguing challenge for the field of eco-hydrology (Porporato & Rodriguez-Iturbe, 2002). A way to meet this challenge is by assessing the impacts of the change in water availability on ecosystems, especially in parts of the world that are highly vulnerable to climatic variability.

Several studies (Boko et al., 2007; Christensen et al., 2007; Müller, Cramer, Hare, & Lotze-Campen, 2011) have shown that P in many

* Corresponding author at: Jet Propulsion Laboratory, California Institute of Technology, USA.
E-mail address: Dimitrios.Stampoulis@jpl.nasa.gov (D. Stampoulis).

http://dx.doi.org/10.1016/j.rse.2016.06.007
0034-4257/

regions in sub-Saharan Africa will change, while others (Faramarzi et al., 2013; Müller, Waha, Bondeau, & Heinke, 2014) show that dry regions will be impacted from climate change more severely than wetter areas, thus posing additional challenges to the crop security of those regions (Fisher et al., 2013; Traore et al., 2014). Overall, there is a consensus that changes in P regimes and frequency of extreme events (Haddeland et al., 2014; Llopart, Coppola, Giorgi, da Rocha, & Cuadra, 2014; Schewe et al., 2014), coupled with an increasing water usage to meet human needs, will fundamentally change water supply in many regions across the globe, with severe implications to the environment, food security, and economic prosperity in many countries (Schewe et al., 2014; Haddeland et al., 2014; Smith et al., 2014; Konar, Jason Todd, Muneepeerakul, Rinaldo, & Rodriguez-Iturbe, 2013; Morrongiello et al., 2011; Arthington, Naiman, Mcclain, & Nilsson, 2010; Vinya, Malhi, Brown, & Fisher, 2012; Vinya et al., 2013). One such example is the water-limited region of East Africa (EA), the countries of which have economies that depend primarily on rain-fed agricultural systems. The extremely complex dynamics of P in this region (Janowiak, 1988; Rodhe & Virji, 1976) exacerbated by the intensification of the hydrological cycle (Durack, Wijffels, & Matear, 2012; Helm, Bindoff, & Church, 2010; Huntington, 2006), often lead to rainfall deficiencies resulting in significant food gaps, impeding national economic performances. In addition, owing to its limited resources for mitigation and adaptation, EA is even more vulnerable to climatic variability, and thus a region of high priority for eco-hydrological studies.

In an effort to explore the relations between the water dynamics and ecosystem processes, several studies (Anyamba, Tucker, & Mahoney, 2002; Armanios & Fisher, 2014; Chen, De Jeu, Liu, Van der Werf, & Dolman, 2014; Davenport & Nicholson, 1993; Deshmukh, 1984; Eklundh, 1998; Nicholson, Davenport, & Malo, 1990; Richard & Poccard, 1998; Shinoda, 1995) have investigated the response of vegetation to P/SM patterns, by examining the spatiotemporal patterns and inter-relations of P/SM and the Normalized Difference Vegetation Index (NDVI) in EA and other sensitive regions of the globe. While spectral vegetation indices, such as NDVI, have been extensively used to analyze spatiotemporal variations in vegetation distribution, their use to quantify vegetation status or behavior is plagued by several shortcomings, such as its high sensitivity to atmospheric influences (cloud, aerosols), constraints due to seasonal decreases in solar illumination, its limitation in monitoring only the top of the canopy (Liu, de Jeu, McCabe, Evans, & van Dijk, 2011), its proneness to saturation in dense canopies (Liu, van Dijk, McCabe, Evans, & Jeu, 2012), and its weak and indirect link with water content (Pettorelli, 2013).

Microwave remote sensing has recently attracted attention as a useful tool for vegetation phenology monitoring. Several studies focus on Vegetation Optical Depth (VOD) retrievals (Table 1), as microwave observations are physically directly related to the water content of the pixels being observed. VOD is a less sensitive to atmospheric effects indicator of both photosynthetic and non-photosynthetic above-ground biomass water content (Jones et al., 2011; Liu et al., 2012; Shi et al., 2008), and it can penetrate vegetation. Moreover, VOD is more sensitive to changes in woody vegetation than in herbaceous overstory, indicating the advantage of its use in monitoring regions with dense or diverse/mixed vegetation cover (Andela et al., 2013). Despite the increasing number of studies focusing on monitoring vegetation phenology, few examine the relations among vegetation dynamics, P, and SM patterns, using microwave remote sensing. SM is the “core of the hydrological cycle” (Eagleson, 1978; Eagleson, 1982; Federer, 1979; Noy-Meir, 1973), and is characterized by a “cause and consequence” relationship with the regional vegetation (Rodriguez-Iturbe, 2000). Moreover, P is the main climatic driver of vegetation dynamics. Therefore, jointly examining the dynamics of vegetation, P, and SM can provide a more holistic and integrated characterization of the regional hydrologic regime.

The current study uses passive microwave remote sensing observations of vegetation water content (VWC) and SM for 2003–2011, provided by WindSat, a satellite-based polarimetric microwave radiometer, to study the behavior of these major attributes under extreme hydrologic conditions, in the highly complex water-stressed region of EA. WindSat was developed by the Naval Research Laboratory primarily to provide the Navy with the much needed ocean surface wind vector measurements; however, it also measures other environmental parameters such as SM and VWC, among others. The spatiotemporal characteristics of sensitivity and resilience of SM and VWC are assessed

Table 1
Overview of studies using passive microwave remote sensing for vegetation phenology monitoring. Studies are ordered chronologically, then alphabetically, and those conducted over the African continent or globally are marked in bold. The current study is added for the sake of completeness.

N	Reference	Passive MW algorithm used for VOD retrieval	Other remote sensing products used for comparison/validation	Region (period of study)	Precipitation jointly assessed	Soil Moisture jointly assessed
1	Liu, de Jeu, van Dijk, and Owe (2007)	TRMM	Not applicable	Australia (1998–2005)	No	Yes
2	**Jones, Jones, Kimball, and McDonald (2011)**	AMSR-E	MODIS VI & LAI	Global (2003–2008)	No	No
3	**Liu et al. (2011)**	SSM/I, TMI, AMSR-E	AVHRR NDVI	Global (1987–2006)	Yes	No
4	Hunt, Li, Yilmaz, and Jackson (2011)	WindSat, MODIS NDII	Not applicable	Central Iowa (2003–2005)	No	No
5	**Guan, Wood, and Caylor (2012)**	AMSR-E	AVHRR NDVI, QuikSCAT σ^0	East-southeastern Africa (1999–2008)	Yes	No
6	Jones, Kimball, Jones, and McDonald (2012)	AMSR-E	MODIS-for-NACP NDVI, LAI	North America (2003–2007)	No	No
7	**Liu et al. (2012)**	SSM/I, TMI, AMSR-E	Not applicable	Global (1988–2008)	No	No
8	**Andela et al. (2013)**	Merged (SSM-I – TMI – AMSR-E)	AVHRR NDVI	Global drylands (1988–2008)	Yes	No
9	Jones, Kimball, Small, and Larson (2013)	AMSR-E	NMRI	Western continental USA & Alaska (2007–2011)	Yes	No
10	Liu et al. (2013)	SSM/I, TMI, AMSR-E	AVHRR NDVI	Mongolia (1988–2008)	Yes	No
11	Van Dijk et al. (2013)	SSM/I, SMMR, TRMM, AMSR-E	MODIS NDVI, AVHRR NDVI	Australia (2001–2009)	Yes	No
12	**Guan et al. (2014)**	AMSR-E	MODIS NDVI	Sub-Saharan Africa (2000 – 2010)	Yes	Yes
13	**Stampoulis, Haddad, and Anagnostou (2014)**	WindSat	QuikSCAT	Madagascar (2003 – 2011)	Yes	Yes
14	**Cui, Shi, Du, Zhao, and Xiong (2015)**	SMOS L1c	MODIS NDVI	Latin America, Africa, Southeast Asia (2010 – 2011)	No	Yes
15	**Current study**	WindSat	MODIS EVI & NDVI	East Africa (2003–2011)	Yes	Yes

during dry spells of different duration. Sensitivity describes the magnitude of the stressing event that the system will resist/absorb without significant change (Holling, 1973; Klaus, Holsten, Hostert, & Kropp, 2011; O'Brien, Leichenko, et al., 2004; O'Brien, Sygna and Haugen, 2004; Römer et al., 2012) and here is assessed by quantifying the relative change. While resilience has several different definitions within the ecological literature (Gunderson, 2000; Harris, Carr, & Dash, 2014), in this paper, it is characterized as the ability, measured in time, to maintain the normal state, or the persistence of the system in maintaining its stability (Holling, 1973). To this end, the primary objectives of this study are to: 1) investigate the inter-relations among the different hydrologic attributes 2) identify and characterize dry spells 3) assess and quantify the hydrologic sensitivity and resilience during dry spells.

2. Study region

2.1. Topography and land use

Equatorial EA (10°N–10°S/30°E–50°E) is the study area encompassing the countries of Ethiopia, Somalia, Kenya, Uganda, Tanzania, and southeastern Sudan. Defined by the Great Rift Valley, EA is characterized by landscapes with high relative relief in close proximity to the ocean (Pik, 2011, Fig. 1). Numerous orographic features of varying sloping relief, large inland lakes, and widely spaced deserts or semi-arid sites make this the most topographically diverse region of the continent (Fig. 1a), with an enormous effect on its climatology (Conway, Allison, Felstead, & Goulden, 2005; Nicholson et al., 1990; Nicholson, 1996).

Fig. 1b shows the different vegetation categories of EA. For the most part, the study area is characterized by forest, woody savanna, savanna, grasslands, and shrublands. Savanna and shrublands occupy 36% and 35% of the study area respectively, while woody savanna regions represent 10% of EA. Grasslands and forested regions account for 8% and 6% of the total area respectively. Other land-cover categories, such as croplands, mixed forest, and barren land occupy smaller regions that appear sporadically in the study area, and therefore only the five aforementioned categories were investigated. Moreover, all analyses for this study were conducted at the ¼ degree spatial and daily temporal resolution, and only 0.25 deg pixels with homogeneous vegetation types were used, to investigate the spatial patterns and characteristics of hydrologic properties for each geographical region of the study area in which a major vegetation type dominates. Land-cover type homogeneity was determined by implementing a threshold value of 60% as the minimum number of the finer resolution land-cover pixels with common vegetation type within each 0.25 deg pixel.

Several geographical and physiological factors enabled grouping of some vegetation categories, for the purposes of this analysis. The entire northeastern region of EA (light- and dark-grey regions, roughly indicated by the red marking in Fig. 1b) is represented by shrublands, and will hereafter be referred to as SHR. Moreover, savannas and grasslands are not only physiologically and phenotypically similar vegetation types (Anderson, Fralish, & Baskin, 2007; McPherson, 1997; Werner, 2009) but they also appear sporadically in the same geographical region, i.e. central and northern Tanzania, roughly indicated by the blue marking in Fig. 1b. Therefore, these two vegetation types, referred to as SG, will be deemed as one category. Furthermore, areas characterized by forest or woody savanna (FWS) always appear in tandem; however, this vegetation regime is represented by two major geographically apart regions, i.e. dark-green and brown regions in central-western Uganda and western Ethiopia, roughly indicated by green circles A and B in Fig. 1b. To examine whether these two regions can be jointly assessed, spatiotemporal analyses of VWC and SM behavior were performed using WindSat VWC and SM observations (Supplementary material S.1). Overall, three major vegetation regimes were defined within EA: FWS, SG, and SHR.

2.2. Climatology

Although EA lies within the tropical latitudes, it exhibits a complex pattern of regional climatic profiles (Nicholson, 1996), owing to the combination of large-scale tropical controls, such as the Intertropical Convergence Zone (ITCZ) that migrates biannually across the region (Nicholson, 1996; Wolff et al., 2011), the existence of lakes, high relative relief, and maritime influences (Nicholson, 2000; Verschuren, Laird, & Cumming, 2000). Because of the ITCZ, parts of the study area experience a bimodal P regime that brings rainy seasons from March to May (namely "long rains") and from October to December (namely "short rains") (Kabanda & Jury, 1999). The bimodal regime, however, changes gradually into a single season with increasing distance from the Equator

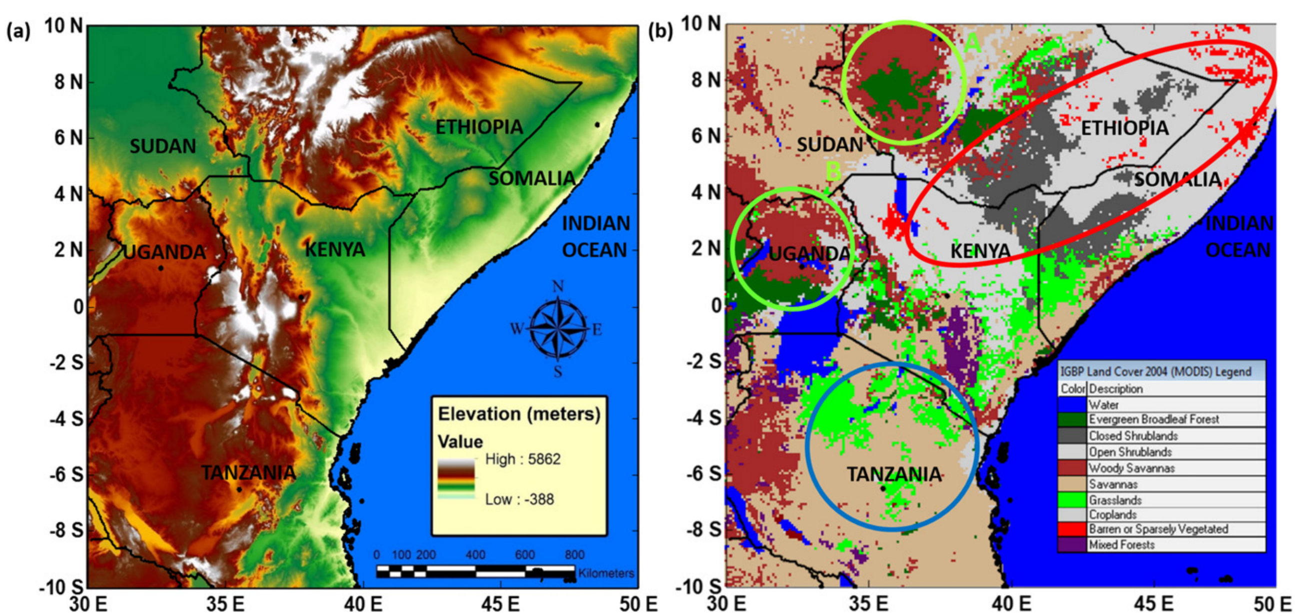

Fig. 1. Maps of (a) topography and (b) land-cover categories in East Africa. In (b) green circles (A and B) correspond to the two distinct regions characterized by Forest/Woody Savanna type of vegetation, the region shown with the red oval-shaped marking indicates Shrublands, and the blue circle marks the area covered by Savanna/Grasslands. (For interpretation of the references to color in this figure legend, the reader is referred to the web version of this article.)

(Conway et al., 2005). The major sources of moisture flux into the region are the monsoonal wind systems, the flow of which is significantly modified inland by the various topographical patterns (Ogallo, 1988), resulting in high spatial and temporal variations in P (Fig. 2a,b).

Similarly, temperature (T) in the region varies greatly in space; Somalia, eastern Kenya, southeastern Ethiopia, South Sudan, and parts of Tanzania are remarkably hotter than the rest of the study domain, while northeastern/northwestern regions are subject to greater temporal T variations (Fig. 2c,d). EA is also characterized by great heterogeneity in VWC (Fig. 2g) and to a lesser extent in SM (Fig. 2e). Temporal variations of VWC and SM also change dramatically in space, indicating that the climatologic landscape of the region is no less variable than its topography (Fig. 2h,f).

3. Data

3.1. Precipitation

The region of EA is characterized by a severe paucity of in-situ P data (Dinku et al., 2007), and thus, the only way to measure P over this topographically complex domain is via remote sensing from space. The satellite P product used in this study is derived from a joint mission between NASA and Japan Aerospace Exploration Agency (JAXA) and named Tropical Rainfall Measuring Mission (TRMM) Multi-satellite Precipitation Analysis (TMPA), specifically 3B42 V7, which is a gauge-adjusted (over land only) product (Huffman et al., 2007). This product is the combination of two sub-products, the microwave and the microwave-calibrated infrared. The final product has a relatively fine spatial (0.25 deg) and temporal resolution (3 hourly), and is available both as post-analysis (3B42 V7) where the 3-hourly passive microwave/infrared estimates are adjusted using monthly gauge comparisons, as well as in real time (3B42 RT) without the gauge correction. The P product used in this study is TMPA 3B42 V7 (covering all areas 50°N–50°S for 1998–2014) at the daily scale and for the 2003–2011 period. Due to the sparseness of gauges in the study region, the estimated P is characterized by relatively high uncertainty (Tian & Peters-Lidard, 2010; Dinku, Ceccato, Cressman, & Connor, 2010; Behrangi, Tian, Lambrigtsen, & Stephens, 2014).

3.2. Vegetation water content and soil moisture

Daily observations of VWC and volumetric SM were provided by the physically-based land algorithm of the NRL's WindSat radiometer for 2003–2011. Its algorithms simultaneously retrieve VWC, SM, and Land Surface Temperature using polarized 10.7-, 18.7-, and 37-GHz channel measurements (Li et al., 2010; Turk, Li, & Haddad, 2014). The algorithm's approach is among the few multichannel algorithms (Njoku, Jackson, Lakshmi, Chan, & Nghiem, 2003; Njoku & Li, 1999; Owe, De Jeu, & Holmes, 2008; Owe, De Jeu, & Walker, 2001) that add the 37-GHz channels. The Single Channel Algorithm (SCA) has also been using the 37 GHz channel to correct for factors that affect the retrieval (Mladenova et al., 2014). Sensitivity studies (Li et al., 2010; Turk et al., 2014) showed that the 37-GHz channels can offer significant SM sensitivities under low vegetation conditions. In another study, Parinussa, Holmes, and De Jeu (2012) derived surface SM from WindSat using C- or X-band brightness temperature observations according to the Land Parameter Retrieval Model (LPRM) and validated the retrieved SM using in situ observations in Europe and Australia; WindSat SM retrieval was found to have a consistent response to changing environmental conditions, consistent temporal behavior, and the ability to capture the daily variation of SM. WindSat automatically accommodates nonlinear transitions, such as that between significant SM sensitivity over desert to high surface temperature sensitivity over vegetated land (Li et al., 2010).

The WindSat land algorithm uses Sensor Data Records resampled to a global cylindrical Equal-Area Scalable Earth Grid (EASE-Grid) (Brodzik & Knowles, 2002) of 25 km for further SDR data processing and land retrieval. The land algorithm bins the swath data onto the EASE-Grid and composes different orbits into separate daily ascending (evening passes) and descending (early morning passes) files. For this study, WindSat data were resampled via (nearest neighbor) interpolation to a regular 0.25 deg grid, and only descending passes were used, to ensure smaller retrieval errors, as the differences between effective land surface and vegetation temperatures are at the daily minimum.

3.3. Land-cover and digital elevation model (DEM)

Vegetation types across EA were identified using the MODIS 2004 land-cover dataset (MCD12Q1), which has 17 classes, defined by the International Geosphere Biosphere Programme (IGBP) classification scheme, and a spatial resolution of approximately 0.004 deg (Friedl et al., 2010). Digital Elevation data (DEM) for the region of EA were provided by the NASA Shuttle Radar Topographic Mission (SRTM) at a 1-km spatial resolution. The DEM was downloaded in Arc-Info ASCII format from the CGIAR Consortium for Spatial Information (CGIAR-CSI) (http://srtm.csi.cgiar.org/).

4. Methods

4.1. Investigating the hydrologic properties of East Africa

The spatial patterns of the similarity among the temporal evolution of daily P, VWC, and SM across EA were assessed by calculating the correlation coefficient (CC) and its statistical significance for each pixel for the investigated time period. Moreover, time series analyses of area-average observations of the aforementioned attributes, as well as their monthly anomalies (Supplementary material S.2), and the CC between each pair of these time series, were performed for each land-cover category for 2003–2011, to characterize the intra-annual and inter-annual temporal patterns of the examined hydrologic variables.

For a qualitative assessment of the inter-relations among the hydrologic attributes and their synchroneity within the various natural ecosystems of EA, all pairs of the above time series were plotted separately for each vegetation type (Supplementary material S.3). Furthermore, for each pixel, the delay in time between two time series was quantitatively assessed by calculating the cross-correlation function (ccf) and the time lag (shift of one hydrologic attribute relative to the other, in the time domain) at which ccf becomes maximum (achieving the highest Pearson Product Moment Correlation). For each pair of investigated variables, positive lag times indicate that the second (first) variable leads (lags) the first (second) one. The results are summarized for the different vegetation regimes and spatial patterns of the aforementioned properties are also discussed.

4.2. Identifying dry spells

To isolate periods of extreme hydrologic conditions in EA within 2003–2011, dry spells of different duration were identified on a pixel-by-pixel basis using P data from TRMM 3B42 V7. The number of dry spells was calculated by identifying, for each 25 km pixel, periods of consecutive days with no or negligible amounts of P (using a daily threshold of ≤0.1 mm). These periods were categorized into short- (10–30 days), moderate- (30–50 days), and long- (exceeding 50 days) duration, and presented as maps. Moreover, the total number of days in dry spell conditions as well as the average numbers and the spatial variability of dry spells for each duration category within each vegetation regime were also calculated.

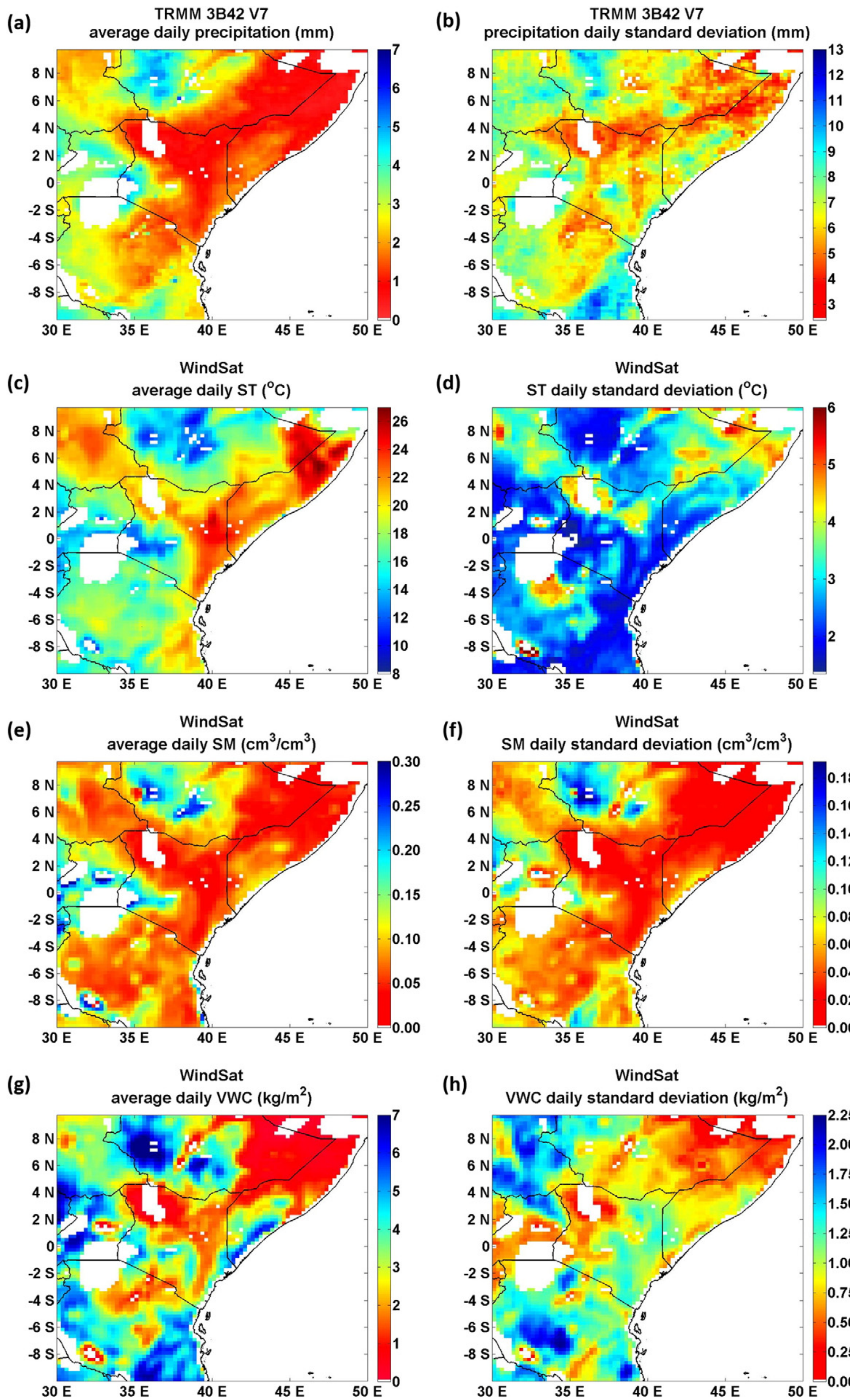
(a)
TRMM 3B42 V7
average daily precipitation (mm)
(b)
TRMM 3B42 V7
precipitation daily standard deviation (mm)
(c)
WindSat
average daily ST (°C)
(d)
WindSat
ST daily standard deviation (°C)
(e)
WindSat
average daily SM (cm³/cm³)
(f)
WindSat
SM daily standard deviation (cm³/cm³)
(g)
WindSat
average daily VWC (kg/m²)
(h)
WindSat
VWC daily standard deviation (kg/m²)
30 E
35 E
40 E
45 E
50 E
8 N
6 N
4 N
2 N
0
-2 S
-4 S
-6 S
-8 S

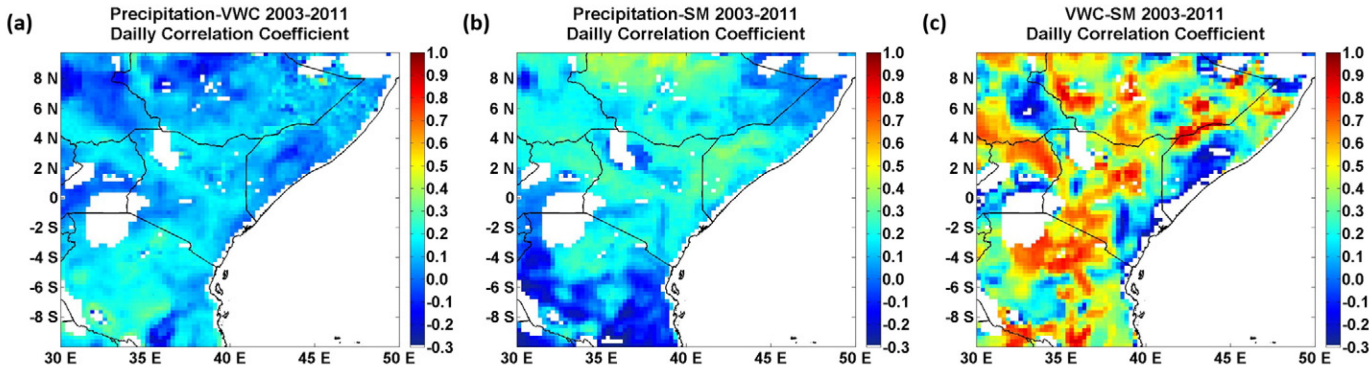

Fig. 3. Maps of daily correlation coefficient for 2003–2011 over East Africa between (a) precipitation and VWC, (b) precipitation and SM, and (c) VWC and SM.

4.3. Assessing hydrologic sensitivity

The sensitivity of the investigated hydrologic attributes is quantified by assessing their relative change under dry spell conditions. The relative change of VWC/SM (symbolized by "X" below) was assessed for all dry spells of each duration category that occurred within each pixel and was calculated based on the following formula:

$$Relative\ \ Change\ \ of\ \ X = \frac{X_2 - X_1}{X_1} \times 100\%$$

where subscript indices 1 and 2 refer to the value of X on the first and last day of a dry spell respectively. The average relative change of X is calculated separately for each dry spell-duration category and for each pixel, and presented as maps, and graphs of space-average values for each vegetation regime and for each dry spell-duration category. Significant differences are presented separately in a table.

4.4. Assessing hydrologic resilience

The VWC/SM resilience was assessed by quantifying, for each dry spell, the number of consecutive days within that period, starting from the first day, during which VWC/SM remained above a specific threshold, normalized by the total dry spell duration. The average value of resilience from all dry spells (regardless of duration) in 2003–2011 was calculated for each pixel and expressed as percentage. Thresholds for both VWC and SM were calculated for each pixel separately based on the 9-year investigated period, and are the 10th, 20th, 30th, 40th, and 50th percentiles of VWC and SM respectively. VWC/SM resilience is presented as maps and graphs (spatially averaged value) to show how this hydrologic property changes among different land-cover categories and for various percentile thresholds. Furthermore, the spatial variability of the VWC/SM resilience in EA was assessed by calculating their standard deviation within each land-cover category and for the different percentile thresholds, and presented as bars. Significant differences are presented separately in a table.

4.5. Statistical analysis

Statistical significance in all differences was assessed by a two-way analysis of variance (ANOVA) followed by a Student-Newman-Keuls multiple comparison test, or by a Student's *t*-test.

5. Results

5.1. Investigating the hydrologic properties of East Africa

We first investigated the inter-relations among the varying P patterns and the VWC/SM dynamics, and how these linkages vary in space. P is generally poorly correlated with VWC and SM, and while P and VWC are more correlated in the southern regions (Fig. 3a), the opposite is true between P and SM (Fig. 3b). In contrast, EA exhibits remarkable spatial heterogeneity in the correlation between VWC and SM dynamics (Fig. 3c), with areas of high and low CCs being intermittently present. More than 82% (91%) of the pixels exhibit significant ($p < 0.05$) CCs between P and VWC (SM), while nearly 96% of the pixels are characterized by significant VWC-SM CCs.

The daily time series of P over EA varies considerably in space and time, among the different vegetation categories (Fig. 4a). FWS regions are subject to a prolonged rainy season (Mar-Sep) followed by a shorter, drier period (Oct–Feb), and this seasonal variability is inter-annually consistent. SG exhibit even higher intra-annual variability in P magnitude, with their wet and dry seasons being inversely correlated with those of the FWS during most of the years. Areas characterized by SHR are subject to an inter-annually consistent bimodal P regime, which brings rainy seasons from March to May and October to December. However, even during the rainy seasons, these regions receive P, the magnitude of which is always lower than that of the other two vegetation regimes. Moreover, the onset and end of the dry periods between the two rainy seasons of each year in SHR coincides almost perfectly with the dry season of SG.

Due to the complex spatiotemporal P patterns, VWC in EA is also highly variable in space and time (Fig. 4b). In FWS, VWC varies seasonally, ranging from 4 to 6 kg/m^2. Peak values appear in October/November followed by a rapid decline reaching the annual minimum in February. In SG, VWC exhibits greater seasonal variations ($> \pm 3\ kg/m^2$) and peak values always precede those of FWS. Moreover, both low and high annual values are lower than the corresponding values of the FWS regions. Even lower lie the VWC values of SHR, where intra-annual variability rarely exceeds 1 kg/m^2. The trend in VWC over these regions is characterized by two major peaks per year.

The SM patterns over EA also exhibit considerable differences among the various land-cover categories (Fig. 4c). Overall, FWS areas experience the highest maximum SM values, while SHR exhibit the lowest maxima. Moreover, FWS regions maintain their SM at values that exceed 0.2 cm^3/cm^3 for long periods of time (April–September). Seasonal variations are larger in FWS (up to 0.28 cm^3/cm^3) and smaller over SG and SHR. Although SHR regions are characterized by a highly irregular pattern of SM with several peaks throughout the year, SG exhibit

Fig. 2. Maps of (left) average and (right) standard deviation values of (a–b) precipitation derived from TRMM 3B42, as well as (c–d) surface temperature, (e–f) soil moisture, and (g–h) vegetation water content, derived from WindSat's respective algorithms over East Africa for 2003–2011.

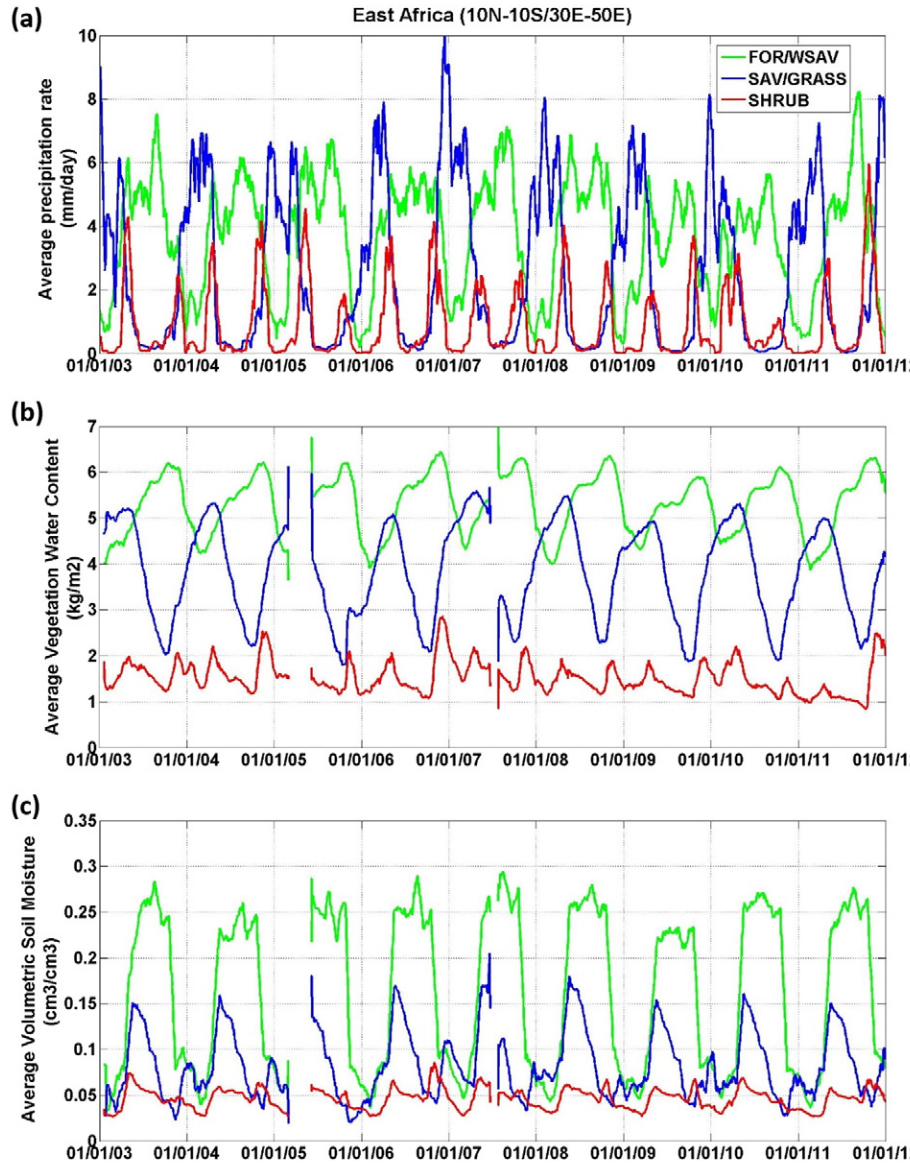

Fig. 4. Time series of the smoothed spatially-averaged daily measurements of (a) precipitation rate, (b) VWC and (c) SM for the three major land-cover categories of East Africa. Gaps in the time series are due to temporary instrument failure.

intermediate seasonal SM fluctuations, with one major peak in April/May and one of lesser magnitude in November.

Table 2 shows the CC (significant at $p < 0.002$) for each pair of spatially-averaged time series of the investigated hydrologic attributes and their monthly anomalies, for each land-cover category. P over FWS is more correlated to SM (0.8) than to VWC (0.42), while the latter two exhibit a CC of 0.6. Correlation between their respective anomalies does not change, except for the P-SM anomalies where their temporal trends agree less than those of P-SM. SG are characterized by better agreement between P and VWC, but very low correlation between P and SM. The anomalies of the latter two however, agree well with each other (0.72). Correlation between P and VWC as well as between VWC and SM exhibit their lowest values over SH, while SG exhibit the highest correlation between P and VWC, and FWS and SHR stand out for their high CC between P and SM. Finally, VWC and SM temporal patterns agree more in FWS, whereas the anomalies of P and SM, as well as those of VWC and SM are well-correlated with each other over all regions.

Spatial patterns of the cross-correlation between P and VWC or SM (Fig. 5a,e) are similar, although values are slightly higher between P and SM. Significantly higher values in both cases are observed over FWS, while the lowest correlations are over SHR (Fig. 5b,f). Cross-correlations between VWC and SM are overall high, with no significant difference among the investigated vegetation categories (Fig. 5I,j). With

Table 2
Correlation coefficients and their significance for each pair of comparison among the three investigated hydrologic variables as well as among their corresponding monthly anomalies, for the three major vegetation regimes in East Africa. All correlation coefficients are significant at $p < 0.002$.

Correlation coefficient	PRECIP-VWC	PRECIP-SM	VWC-SM	PRECIP ANOM-VWC ANOM	PRECIP ANOM-SM ANOM	VWC ANOM-SM ANOM
FWS	0.42	0.80	0.60	0.42	0.46	0.60
SG	0.54	−0.27	0.43	0.37	0.72	0.64
SHR	0.37	0.57	0.31	0.31	0.68	0.68

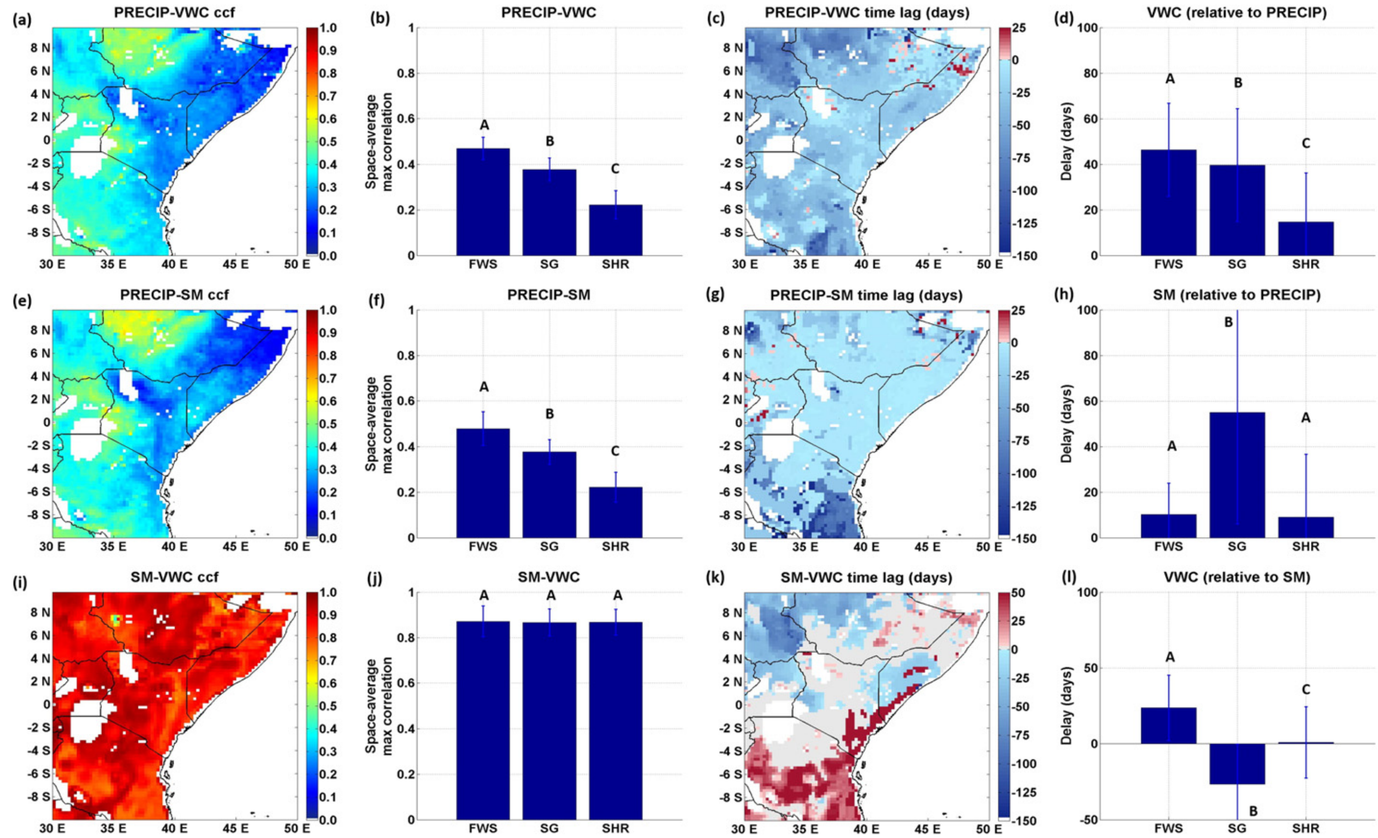

Fig. 5. Maximum correlation coefficient calculated from the cross-correlation function shown as (a,e,i) maps and (b,f,j) space-average values for the three major vegetation classes, and time lag at which maximum correlation was obtained, presented as (c, g, k) maps and (d, h, l) space-average values for the three major land-cover categories between (a–d) precipitation and VWC, (e–h) precipitation and SM, and (i–l) SM and VWC. Scale on the color bar and y-axis is not the same among maps c, g, k and bar plots d, h, l respectively. Error bars represent standard deviation. Columns in bar plots marked by different letters are significantly different as determined by a one-way ANOVA followed by a Student-Newman-Keuls multiple comparison test. (For interpretation of the references to color in this figure legend, the reader is referred to the web version of this article.)

regards to time lags, P leads VWC over most of the study area, as indicated by the negative values (Fig. 5c). Specifically, northern and southern regions exhibit greater time lags (>40 days) than Equatorial or eastern regions. A few, smaller in area, regions in northeastern EA are characterized by positive time lags, indicating that VWC leads P; this could be attributed to potential major lateral inflow events, or perhaps missed P events by TRMM. VWC lag times vary significantly among the three categories (Fig. 5d); the longest lag is observed in FWS (>45 days) and the shortest in SHR regions (note: negative time lag values in maps c, g, and k are presented as positive values in bar plots d, h, and l). Similarly to VWC, P also leads SM over most of EA (Fig. 5g). FWS or SHR exhibit short SM lag times (<10 days), while significantly longer delays (>55 days) are observed in SG (Fig. 5h). Finally, there is a delay of VWC with respect to SM in FWS and SHR, while the opposite is true over SG (Fig. 5k). Central/northeastern regions, including areas covered by SHR, are characterized by zero delays between VWC and SM. Overall, at the vegetation regime level, SM leads VWC in FWS and, at a marginal level, in SHR, but it lags VWC in SG (Fig. 5l).

5.2. Identifying dry spells

The spatial patterns of the total number of dry spells for each duration category (Fig.6a–c), indicate that each region in EA is subject to a unique series of dry spells that vary in duration. Most of the short- and moderate-duration dry spells occur in the central and coastal regions of EA, with similar patterns; however, the frequency of the latter is considerably lower than that of the former. With regards to long-duration dry spells, eastern regions are severely plagued by them, while South Sudan is also prone to extended periods of P deficiency, but to a lesser extent. By and large, regardless of duration, central and coastal regions of EA are more frequently subject to dry periods (Fig. 6d). Investigating the differences in the average number of dry spells among the different vegetation regimes and the three dry spell duration categories (Fig. 6e) reveals a generally decreasing trend with increasing dry spell duration, except for SHR, where the number of long dry spells is significantly higher than that of moderate ones, consisting 35% of the total number of dry spells. Total number of days under dry spell conditions in 2003–2011 also varies substantially across the study domain (Fig. 6f); eastern and, to a lesser extent, southeastern regions experience the highest numbers of days with no P. More than 90% of the 2003–2011 period in certain regions in Somalia or southeastern Ethiopia, is under dry spell conditions.

5.3. Assessing hydrologic sensitivity

Fig. 7 presents the sensitivity of VWC and SM to dry spells of different duration and for the major vegetation regimes of EA. During short dry spells, VWC relative change (hereafter also referred to as "change") is characterized by both negative and positive values within each vegetation type, ranging from −70% to several cases that exceed +100% (Fig. 7a), whereas the vegetation behavior during moderate dry spells is more uniform in space (Fig. 7b), with negative values dominating, although there are regions in SHR/SG that still exhibit positive values. However, during the long stress-inducing dry spells, although VWC is generally characterized by varying decreasing trends, a relatively large region in the northeast is subject to a substantial VWC increase or uptake (Fig. 7c). Overall, VWC in regions characterized by FWS/SG follows a generally decreasing trend, which becomes more pronounced with increasing dry spell duration (Fig. 7d). Conversely, although SHR are characterized by an increase in the magnitude of VWC release when dry

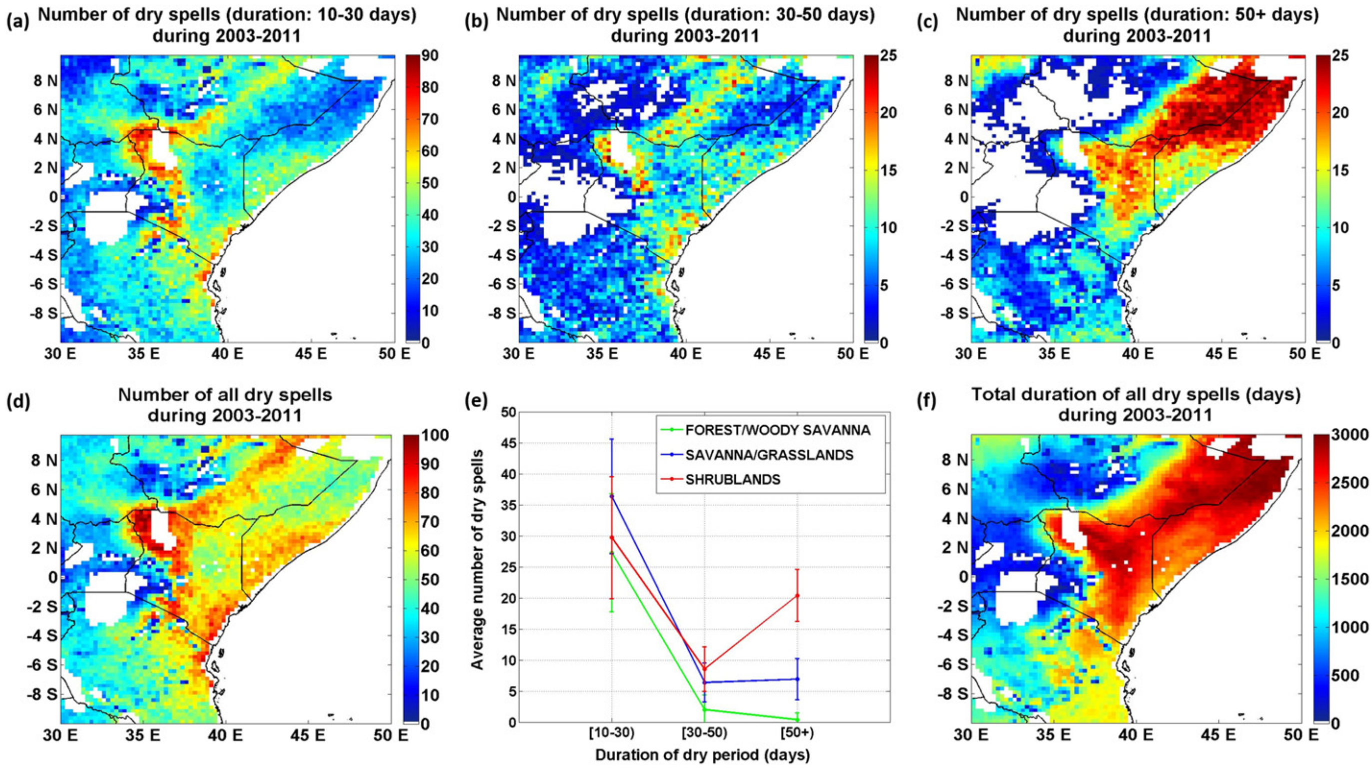

Fig. 6. Maps of dry spell occurrence in East Africa for (a) short-duration, (b) moderate-duration and (c) long-duration dry spells. Scale on the colorbar is not the same among the maps. Map (d) shows the total number of dry spells of all duration categories. Graph (e) presents the space-average number of dry spells for each vegetation regime and for the three duration categories. Error bars represent standard deviation. Map (f) shows the total number of days in dry spells during 2003–2011.

spell duration increases from short to moderate, during long dry spells their VWC dynamics change significantly (Table 3) not only in magnitude, but also in nature, as a substantial number of pixels exhibit positive values. Spatial variability of VWC change is low (high) in FWS (SHR), while in SG it increases with dry spell duration (Fig. 7d). All differences within the same vegetation regime and within the same dry spell duration-category are significant, except for the long-duration dry spell, during which only SHR are significantly different than the other vegetation types (Table 3).

With regards to SM relative change during dry spells, varying spatial patterns are observed, especially during short dry spells (Fig. 7e), where southern and, to a lesser extent, northeastern regions exhibit a positive change of SM, despite the lack of P. With increasing duration of dry spells, SM change increases in magnitude with negative values dominating in a more spatially uniform fashion (Fig. 7f,g). By and large, the decrease of SM in all vegetation regimes intensifies with increasing duration of dry spells. However, the overall trends of the three investigated vegetation categories differ markedly (Fig. 7h); FWS consistently

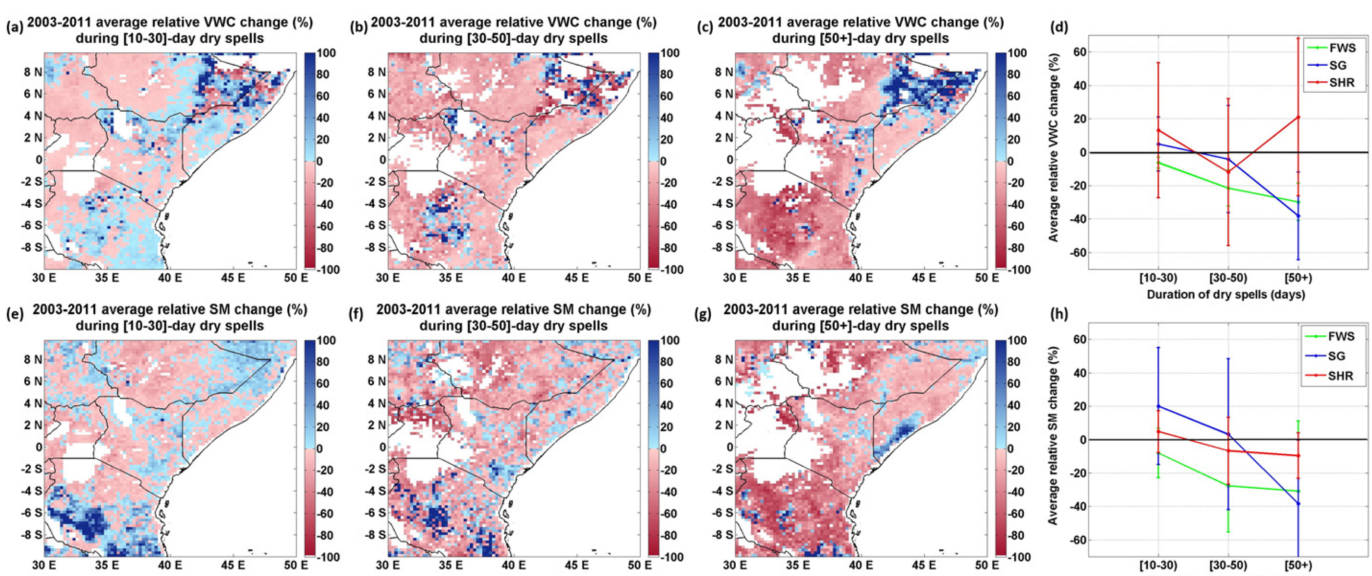

Fig. 7. Sensitivity of (a–d) VWC and (e–h) SM in East Africa during dry spells. From left to right, maps show the relative VWC/SM change during short-, moderate-, and long-duration dry spells. Graphs (d) and (h) show the average relative VWC and SM change respectively for each vegetation regime and for the three dry spell duration categories. Error bars represent standard deviation.

Table 3
Significant differences in the sensitivity of VWC and SM during dry spells within the same vegetation regime (upper case letters) as well as within each dry spell duration category (lower case letters). Different letters indicate significant difference, as determined by a one-way ANOVA followed by Student-Newman-Keuls multiple comparison test.

	Duration of dry spells (days)	VWC relative change	SM relative change
FWS	[10–30)	Aa	Aa
	[30–50)	Ba	Ba
	[50+)	Ca	Ba
SG	[10–30)	Ab	Ab
	[30–50)	Bb	Bb
	[50+)	Ca	Cb
SHR	[10–30)	Ac	Ac
	[30–50)	Bc	Bc
	[50+)	Cb	Cc

exhibit negative values during all dry spells, while SHR are characterized by a small SM increase during short dry spells and a small decrease during moderate periods without P, which is intensified during long periods without rainfall. Moreover, although SM in SG does not seem to be negatively affected by short dry spells, its overall change, although still positive, is significantly (Table 3) reduced during moderate dry spells. However, a markedly negative impact on SG SM is evident during long dry spells. A point to note is that during both short and long dry spells, SG are characterized by the highest in magnitude SM change, with positive and negative values respectively, thus exhibiting the most extreme behavior. In addition, SG (SHR) exhibit the greatest (lowest) variability in their SM response during all dry spells.

5.4. 5.4. Assessing hydrologic resilience

Maps of VWC resilience during dry spells for various thresholds are presented in Fig. 8. For the lowest VWC threshold (≥10th percentile) most of EA exhibits high (90–100%) resilience, with areas in northern Uganda and western Tanzania characterized by relatively lower resilience; however, a substantial number of pixels in SHR, present markedly lower resilience, and these patterns are maintained throughout all investigated VWC thresholds. Unsurprisingly, resilience generally decreases with increasing threshold (Fig. 8b–e), except for the regions in northern Somalia and southeastern Ethiopia which exhibit low resilience regardless of the threshold used.

Spatial patterns of SM resilience are not similar to those of VWC resilience (Fig. 9). For the lowest SM threshold (Fig. 9a) resilience is overall high, especially in FWS/SG. SHR exhibit relatively high resilience with little spatial variation. However, as the SM threshold increases, resilience not only decreases, but is also characterized by markedly different spatial patterns. Overall, SHR and SG exhibit a gradual decrease in their SM resilience. However, this is not the case with the northwestern regions of EA; these areas are subject to varying rates of changes in the SM resilience with increasing thresholds. Specifically, while some pixels in this region exhibit a gradual decrease in their soil's capacity to maintain its water content, some others display very abrupt changes in their SM resilience during dry spells, thus indicating a rapid loss of SM. These facts indicate a very diverse soil behavior in EA. Generally, and for the 30th, 40th, and 50th percentiles, southern and, to a lesser extent, eastern regions are characterized by higher SM resilience.

In Fig. 10 we describe how VWC (a) and SM (b) resilience during dry spells change among the three major vegetation types of EA and the various percentile thresholds, as well as how these properties vary in space (c and d). Overall, VWC (SM) resilience decreases with increasing VWC (SM) thresholds, and while SHR regions exhibit the lowest (highest) VWC (SM) resilience for all thresholds, SG (FWS) and to a lesser extent FWS (SG), have the most (less) resilient VWC (SM). Resilience is higher for SM than for VWC in SHR and SG, while the opposite is true for FWS. All differences in the VWC/SM resilience are significant (Table S2 in Supplementary material S.4).

There are remarkable discrepancies in the spatial variability of VWC/SM resilience for each percentile threshold among the investigated vegetation regimes. VWC resilience varies more (less) in space within SHR (FWS and SG) regions (Fig. 10c). These patterns are true for all VWC thresholds, and the variation in the VWC resilience decreases with

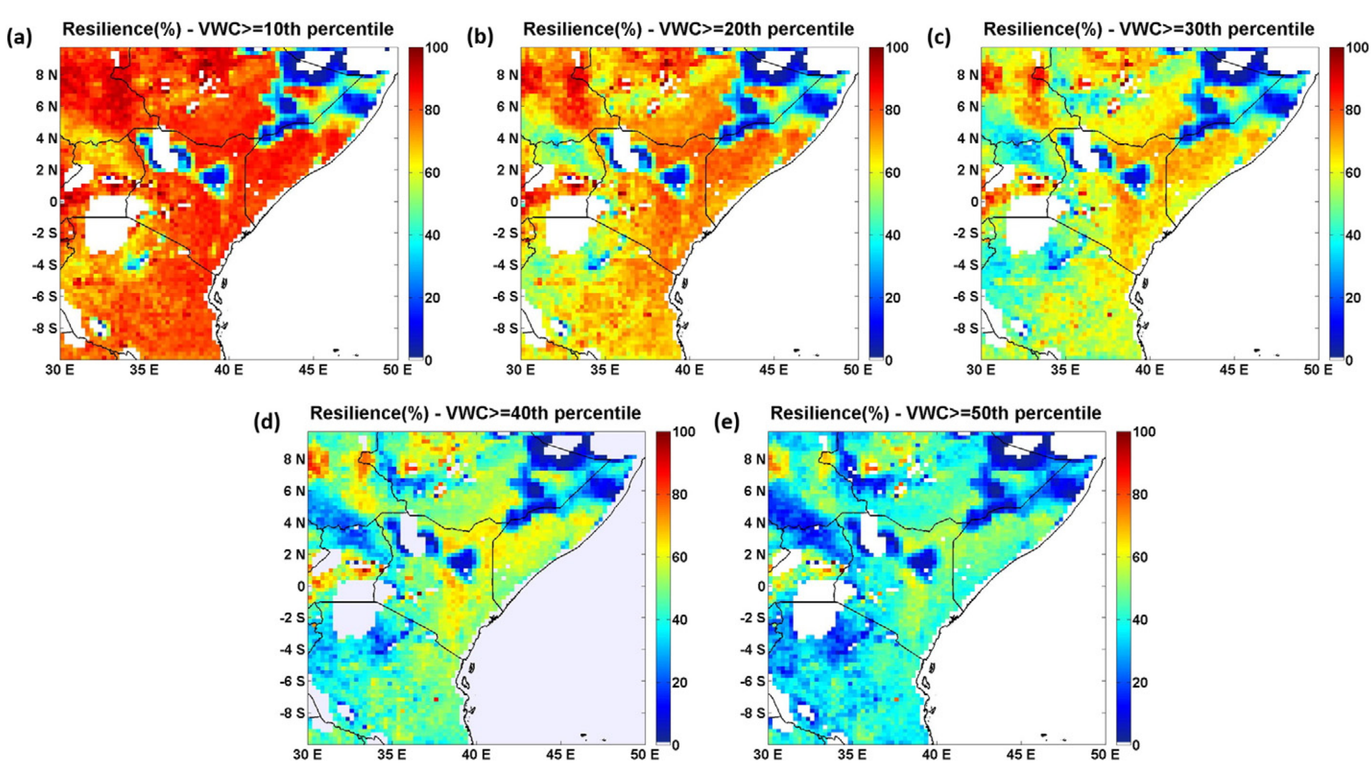

Fig. 8. Maps of average VWC resilience, calculated as the number of consecutive days, within each dry spell, during which VWC remained above a specific threshold, and normalized by the total dry spell duration. The average value of resilience from all dry spells in 2003–2011 was calculated for each pixel and expressed as percentage. VWC thresholds were calculated for each pixel separately based on the 9-year investigated period, and are the 10th, 20th, 30th, 40th, and 50th percentiles of VWC.

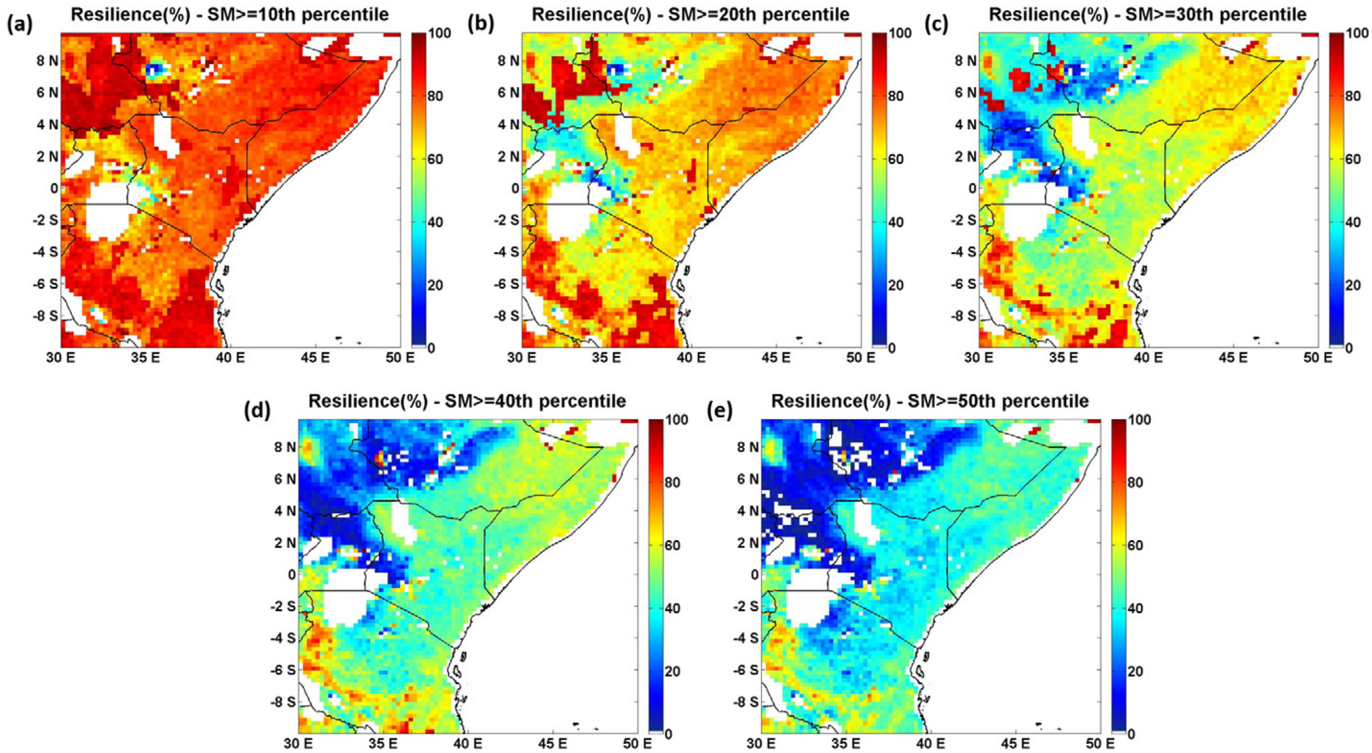

Fig. 9. Same as in Fig. 8, but for SM.

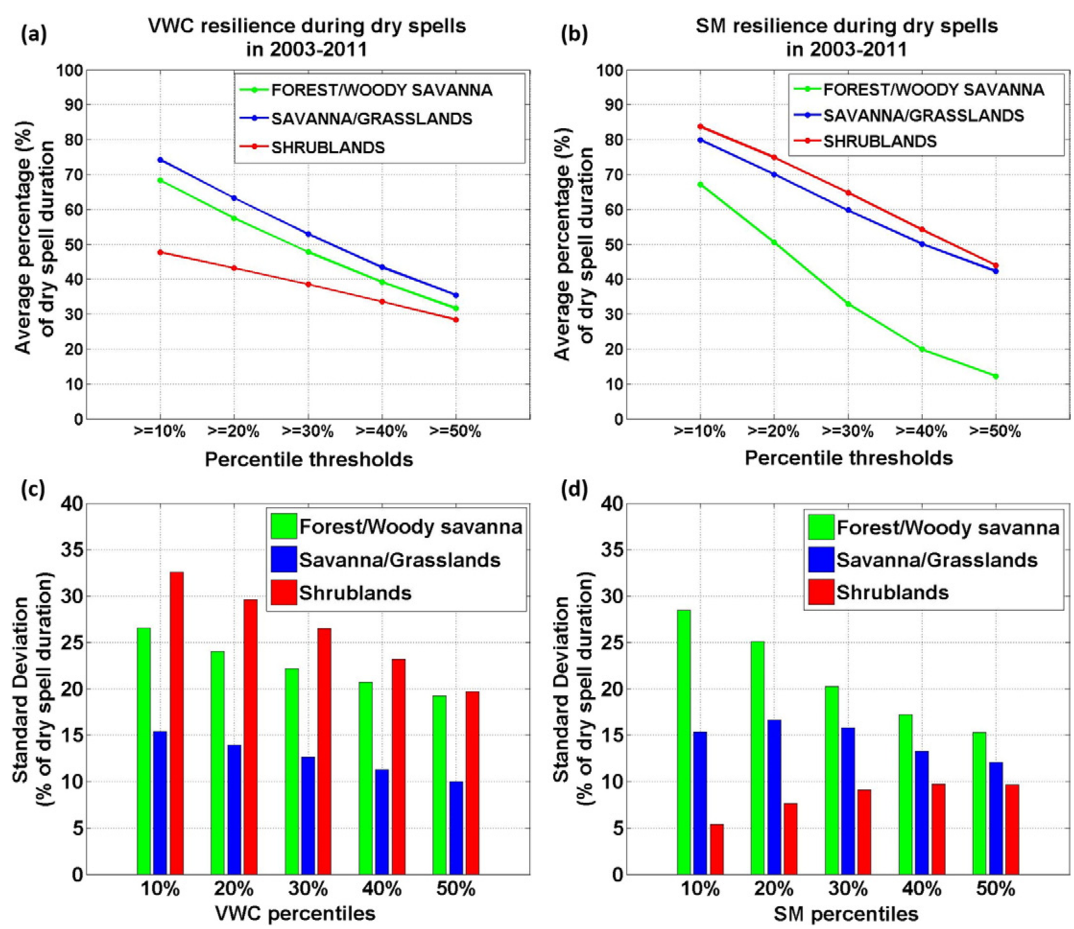

Fig. 10. Resilience of (a) VWC and (b) SM, defined as the average percentage of duration of all dry spells, during which VWC/SM remained above various thresholds, normalized by the total dry spell duration, presented for the three major vegetation regimes of East Africa and the examined percentile thresholds. Standard deviation of the (c) VWC and (d) SM resilience within each land-cover category and for the different thresholds.

increasing threshold in all regions. This, however, is not always the case with the variability of SM resilience; variation in the SM resilience decreases with increasing thresholds in FWS and, for the most part, SG, but the opposite is true in SHR (Fig. 10d). Overall, SM resilience varies more in FWS and SG, while SHR exhibit the lowest variation for all thresholds.

6. Discussion

6.1. Investigating the hydrologic properties of East Africa

The very complex hydro-climatic profile of EA is illustrated by the low CCs between P and VWC/SM which emphasize the need to investigate the relations between water dynamics and ecosystem processes in this geographical region. Moreover, the mosaic of regions with high- and low- VWC-SM CCs within EA indicates the presence of different soil types within areas of the same land-cover category, and therefore various micro-climatic conditions. In addition, the time series and spatial patterns of the three investigated hydrological attributes revealed the multitudinous climatological landscape of EA. Each of the investigated land-cover types exhibits its own hydrologic properties with uniquely different intra- and inter-annual patterns of P, VWC, and SM, thus responding differently to local hydrologic extremes. The varied degree of correlation of the three aforementioned variables among the investigated vegetation regimes indicates remarkable differences in the interrelations among the major hydrologic components of these natural habitats, which likely impact local ecosystem behavior, and ultimately the biotic composition of the region.

With regards to the synchroneity among the investigated hydrologic attributes, SHR are characterized by the least direct response of VWC/SM to the temporal variations of P (lowest cross-correlations), while the opposite is true for FWS. Vegetation response time to P patterns is substantially longer in densely vegetated regions, and decreases as the land-cover type changes to the sparsely vegetated SHR. With regards to the SM response to P, rainfall leads SM over FWS and SHR regions with similar lag times (approx. 10 days), whereas for SG, SM delay is dramatically longer and with very high spatial variability. Evidently, the feedbacks between SM and P in SG differ from those in other regions of EA, potentially due to their unique climatological conditions. Generally, these feedbacks can be either positive (enhancing P persistence) or negative (suppressing P) (Brunsell, 2006; Jones & Brunsell, 2009; Guillod et al., 2015). With respect to the VWC-SM relationship, time lags differ markedly among the three vegetation regimes. Regions covered by FWS and SHR are characterized by leading SM with average time lags of 23 and 2 days respectively; however, SM lags VWC in SG by approximately 25 days. It should be noted that SG exhibit an extremely large spatial variability in the SM-VWC lag times, as this region is characterized by zero-, negative-, and positive-lag sites, indicating a high level of complexity in the VWC-SM relationships. The high spatial variability of time lags in SG could potentially be due to differences in water table depth (Supplementary material S.3), major lateral inflow events that could be altering the hydrological profile of this ecosystem, or different biophysical characteristics, such as shallow rooting depth and seasonal phenology leading to fast water uptake and rapid SM depletion (Liu, Notaro, & Gallimore, 2010). Moreover, conducting the same analysis over the entire sub-Saharan Africa showed that the differences in the relation between VWC and SM are dictated by the various climatic zones of the continent (Supplementary material S.3).

Evidently, the delay with which VWC responds to the P forcing in EA varies significantly in space. Interestingly, regions with long time lags are associated with significant amounts of P, whereas regions characterized by shorter time lags receive remarkably less rainfall. Furthermore, SM responds to P in a more complicated fashion, lagging P over all regions, but with remarkably longer lag times in SG. Finally, high maximum CCs characterize the relationship between VWC and SM throughout the entire study domain with no significant differences among the three land-cover categories, but with time lags that vary dramatically in space, indicating unique regional microclimatologies. By and large, the spatial variability of time lags is always larger within SG and SHR, suggesting a high level of complexity/diversity in these regions. All the above corroborate the fact that the very complex hydroclimatology of EA has a markedly confounding effect on the biome distribution in the area (D'Odorico & Bhattachan, 2012; Grimm et al., 2013).

6.2. Assessing hydrologic sensitivity

Maps of hydrologic sensitivity over EA yielded significant information on the spatial patterns of VWC and SM response during periods without P. The relative change of VWC during dry spells is characterized by a spatially very diverse behavior, with FWS/SG regions exhibiting a distinct VWC decay pattern of increasing magnitude with increasing dry spell duration. FWS is more susceptible to P deficits during short and moderate dry spells, while SG is more adversely affected during long dry spells. Losses, however, of VWC in SHR during periods without P are present only during moderate dry periods, as during the short and, surprisingly, the long stress-inducing dry spells, vegetation in these regions exhibits a remarkable increase in its water content. Common characteristic in SG and SHR is the fact that within both vegetation regimes there are considerable numbers of pixels indicating that vegetation is either locally adversely affected or substantially enriched in water content during all dry spell duration categories, while spatial heterogeneity is markedly lower in FWS regions.

Change of SM during dry spell is also characterized by significant spatial variability across the study area, although the non-uniform behavior of SM diminishes as the duration of dry spells increases. By and large, SM decay increases with increasing duration of dry spells, and this is true for all vegetation regimes. However, SM response in SG follows a uniquely different pattern, with a stronger positive (negative) impact during short (long) dry spells; this behavior indicates that although SM in these regions is not impacted during short (and moderate) deviations from the regional average hydrologic patterns, it undergoes severe changes during long periods with no P. Moreover, the change of SM in SHR is spatially more uniform compared to SG and FWS.

In terms of hydrologic sensitivity, SHR clearly stand out among the three examined vegetation classes, as VWC in these regions was the least impacted by dry spells, especially during short and long dry spells. The positive values of VWC change during the aforementioned dry periods indicates the existence of regions that exhibit tolerance of various levels to dry spells; this could be attributed to the fact that the investigated vegetation type potentially undergoes significant physiological changes during prolonged dry spells, which increase the vegetation's capability of retaining (or even increasing) its moisture content and therefore, maintaining its productivity/status at high levels. Considering the passive microwave-based retrieval's sensitivity to VWC of both leafy and woody components, one can assume that this behavior is characteristic of xerophytic vegetation that can sustain long periods of drought conditions without signs of wilting (Andela et al., 2013; Khamis & Papenbrock, 2014). On the other hand, patterns of SM change indicate lower sensitivity for SG and, to a lesser extent SHR, during short and moderate dry spells, while during long dry spells, SHR are the least impacted regions, suggesting an extended resistance to P deficiency. During short and moderate dry spells, FWS experience the greatest negative impact, while during extensive periods with no P, SG exhibit the highest sensitivity.

All in all, considering all dry spells, SHR are characterized by the lowest average VWC and SM relative change, indicating high vegetation resistance and a more uniform and widely consistent behavior of SM during periods of extreme hydrologic conditions. Low SM sensitivity in these regions could be due to a potential synergistic relationship, with reciprocal effects, between the existing (xerophytic) vegetation and the soil type(s) that support(s) it. The remarkably low hydrologic sensitivity of SHR to dry spells, results in the sustained existence of mesic environmental conditions, and thus, allowing the vegetation to maintain its productivity relatively constant throughout the year. These local micro-climatic conditions ultimately affect the region's biotic composition and biodiversity.

6.3. Assessing hydrologic resilience

The complex dynamics of vegetation and SM in EA are well illustrated by the maps of hydrologic resilience. Within the greater region of the study domain, there is a number of areas characterized by high VWC resilience but low SM persistence. The opposite is true for several other regions. Furthermore, the aforementioned discrepancies are not consistent among the various investigated thresholds, as VWC/SM resilience change remarkably not only in magnitude, but also at different rates, with increasing thresholds. While most of the study area exhibits a gradual decrease in VWC resilience as the threshold increases, certain regions in SHR (specifically in northern Somalia and southeastern Ethiopia) are characterized by vegetation with a remarkably low capacity to maintain its water content during periods of P deficiency. However, SM in these regions presents relatively high persistence in maintaining its stability. Taking into account that 1) the entire Shrublands region is covered by the same type of vegetation 2) all of this area is subject to the same precipitation regime (Fig. 2a), and 3) SM resilience is relatively spatially uniform across the entire SHR domain, the differences in the persistence of vegetation during dry periods can be largely attributed to the existence or lack of relatively shallow groundwater that can sustain these deep-rooted xerophytic plants (supporting analysis in Supplementary material S.5). Shrublands consist of plants that are known for their roots' ability to penetrate through deeper soil layers (Le Maitre, Scott, & Colvin, 1999), and as such, the presence of a shallow groundwater table that reaches the root zone, can sustain the local vegetation in the region even during long non-rainy seasons. Indeed, there is a large body of evidence that suggests that water table depth controls to a large extent the spatial distribution of niches, sorting vegetation (Fan, Li, & Miguez-Macho, 2013; Le Maitre et al., 1999; Orellana, Verma, Loheide, & Daly, 2012; Robinson et al., 2008; Rossatto, Silva, Villalobos-Vega, Sternberg, & Franco, 2012) or even driving physiological adaptation within a given species (Orellana et al., 2012).

Regions in the northwestern parts of EA lose their capacity to retain their SM much faster than they do the same for VWC. Moreover, regions covered by SHR exhibit the lowest (highest) VWC (SM) resilience, while resilience in FWS is higher for VWC than SM. SG on the other hand present similar tolerance levels for both VWC and SM. VWC resilience exhibits higher values of spatial variability in SHR and SG than in FWS. Furthermore, regions of the same vegetation regime with low average resilience are usually also characterized by high spatial variability. High variability in the VWC/SM resilience could be attributed to several potential reasons: different floral composition with various morphological/anatomical characteristics responsible for their respective ability to resist to water stress, vegetation-atmosphere-soil dynamics that vary significantly in space and time, the existence of different soil types, varying duration and intensity of SM depletion, spatial variations of groundwater level, as well as the highly variable atmosphere's water demand. However, recognizing the limitation of the SM retrieval (X-band) which only refers to the surface soil layer, this difference in spatial patterns between VWC and SM resilience would probably be of a lesser extent if WindSat could retrieve rootzone SM, and this is because VWC and SM in the rootzone are highly correlated, and any deviation of one changes the other.

7. Conclusion

We used microwave remote sensing observations of P, SM, and VWC for the 2003–2011 period to assess the hydro-ecological vulnerability of different habitats in EA under extreme hydrologic conditions. The results of this study illustrate the extremely complex hydro-climatic profile of this water-stressed region, which has led to the presence its unique biomes. Regions covered by dense vegetation cover (FWS) or more hydric, mesic vegetation types (SG) are more sensitive to local hydrologic extremes, while xerophytic vegetation (SHR) and the soils that support it are the least impacted by these conditions. However, SG and FWS exhibit the highest VWC resilience, whereas soils in SHR/SG are characterized by the highest capacity of retaining their moisture content during dry spells. Moreover, SHR/SG exhibit great spatial variability in their hydrologic sensitivity, while SHR/FWS are characterized by the highest spatial variability in terms of resilience, indicating that resilience can potentially be locally enhanced by environmental variability and high levels of biodiversity, thus supporting the diversity-stability hypothesis (Ives & Carpenter, 2007; McCann, 2000) according to which, these ecosystems can resist disturbance and/or recover rapidly from a perturbation.

These findings emphasize the paramount importance to assess both hydrologic sensitivity and resilience to provide an integrated understanding of the inter-relations among the various hydrologic components of natural ecosystems, and therefore, a more holistic assessment of their hydrologic vulnerability. Furthermore, despite the varying vegetation and climatic conditions of this complex region and the large footprints of passive microwave radiometers, very useful information from a hydro-ecologic perspective can be extracted from existing radiometric sensors. This information can, in turn, be used towards advancing management and decision support systems that would improve societal well-being, economic development, and food security.

Further analyses, including the use of other remote sensing products regarding surface hydrologic properties (e.g. normalized radar cross section, evapotranspiration), can reveal more information about the dynamics of different ecosystem processes, and provide a more integrated understanding of plant and ecosystem responses and behavior during extreme hydrologic conditions, which will undoubtedly lead to a more sustainable management of water and carbon resources in future climates.

Acknowledgements

The research was carried out at the Jet Propulsion Laboratory, California Institute of Technology, under a contract with the National Aeronautics and Space Administration. This work was supported by NASA Research Announcements (NRA) NNH11ZDA001N-SERVIR. We also acknowledge and appreciate Dr. Li Li from the Naval Research Laboratory (NRL) for providing the WindSat VWC and SM data, as well as the Associate Editor and the three anonymous reviewers for their constructive criticism that helped us greatly improve this manuscript.

Appendix A. Supplementary data

Supplementary data to this article can be found online at http://dx.doi.org/10.1016/j.rse.2016.06.007.

References

Andela, N., Liu, Y. Y., van Dijk, A. I. J. M., de Jeu, R. A. M., & McVicar, T. R. (2013). Global changes in dryland vegetation dynamics (1988–2008) assessed by satellite remote sensing: Comparing a new passive microwave vegetation density record with reflective greenness data. *Biogeosciences*, *10*(10), 6657.

Anderson, R. C., Fralish, J. S., & Baskin, J. M. (2007). *Savannas, barrens, and rock outcrop plant communities of North America*. Cambridge University Press.

Anyamba, A., Tucker, C. J., & Mahoney, R. (2002). From El Niño to La Nina: Vegetation response patterns over east and southern Africa during the 1997–2000 period. *Journal of Climate*, *15*(21), 3096–3103.

Armanios, D., & Fisher, J. B. (2014). Measuring water availability with limited ground data: An entirely remote sensing-based hydrologic budget model of the Rufiji Basin, Tanzania using TRMM, GRACE, MODIS, SRB and AIRS. *Hydrological Processes*, *28*(3), 853–867.

Arthington, Á. H., Naiman, R. J., Mcclain, M. E., & Nilsson, C. (2010). Preserving the biodiversity and ecological services of rivers: New challenges and research opportunities. *Freshwater Biology*, *55*(1), 1–16.

Asbjornsen, H., Goldsmith, G. R., Alvarado-Barrientos, M. S., Rebel, K., Van Osch, F. P., Rietkerk, M., ... Dawson, T. E. (2011). Ecohydrological advances and applications in plant–water relations research: A review. *Journal of Plant Ecology*, *4*(1–2), 3–22.

Behrangi, A., Tian, Y., Lambrigtsen, B. H., & Stephens, G. L. (2014). What does CloudSat reveal about global land precipitation detection by other spaceborne sensors? *Water Resources Research*, *50*(6), 4893–4905.

Boko, M., Niang, I., Nyong, A., Vogel, C., Githeko, A., Medany, M., ... Yanda, P. (2007). Africa. In M. L. Parry (Eds.), *Climate change 2007: Impacts, adaptation and vulnerability. Contribution of working group II to the fourth assessment report of the intergovernmental panel on climate change* (pp. 433–467). Cambridge UK: Cambridge University Press.

Brodzik, M. J., & Knowles, K. W. (2002). *EASE-grid: A versatile set of equal-area projections and grids.* (Discrete Global Grids).

Brunsell, N. A. (2006). Characterization of land-surface precipitation feedback regimes with remote sensing. *Remote Sensing of Environment*, *100*(2), 200–211.

Chen, T., De Jeu, R., Liu, Y. Y., Van der Werf, G. R., & Dolman, A. J. (2014). Using satellite based soil moisture to quantify the water driven variability in NDVI: A case study over mainland Australia. *Remote Sensing of Environment*, *140*, 330–338.

Christensen, J. H., Hewitson, B., Busuioc, A., Chen, A., Gao, X., Held, I., ... Whetton, P. (2007). Regional climate projections. In S. Solomon (Eds.), *Climate Change 2007: The physical science basis. Contribution of working group I to the fourth assessment report of the intergovernmental panel on climate change* (pp. 849–940). Cambridge United Kingdom and New York, NY, USA: . Cambridge University Press.

Conway, D., Allison, E., Felstead, R., & Goulden, M. (2005). Rainfall variability in East Africa: Implications for natural resources management and livelihoods. Philosophical Transactions of the royal society A: Mathematical. *Physical and Engineering Sciences*, *363*(1826), 49–54.

Cui, Q., Shi, J., Du, J., Zhao, T., & Xiong, C. (2015). An approach for monitoring global vegetation based on multiangular observations from SMOS. *IEEE Journal of Selected Topics in Applied Earth Observations and Remote Sensing*, *8*(2), 604–616.

Davenport, M. L., & Nicholson, S. E. (1993). On the relation between rainfall and the normalized difference vegetation index for diverse vegetation types in East Africa. *International Journal of Remote Sensing*, *14*(12), 2369–2389.

Deshmukh, I. K. (1984). A common relationship between precipitation and grassland peak biomass for east and southern Africa. *African Journal of Ecology*, *22*(3), 181–186.

Dinku, T., Ceccato, P., Cressman, K., & Connor, S. J. (2010). Evaluating detection skills of satellite rainfall estimates over desert locust recession regions. *Journal of Applied Meteorology and Climatology*, *49*(6), 1322–1332.

Dinku, T., Ceccato, P., Grover-Kopec, E., Lemma, M., Connor, S. J., & Ropelewski, C. F. (2007). Validation of satellite rainfall products over East Africa's complex topography. *International Journal of Remote Sensing*, *28*(7), 1503–1526.

D'Odorico, P., & Bhattachan, A. (2012). Hydrologic variability in dryland regions: Impacts on ecosystem dynamics and food security. *Philosophical Transactions of the Royal Society B: Biological Sciences*, *367*(1606), 3145–3157.

Donohue, R. J., Roderick, M. L., McVicar, T. R., & Farquhar, G. D. (2013). Impact of CO2 fertilization on maximum foliage cover across the globe's warm, arid environments. *Geophysical Research Letters*, *40*(12), 3031–3035.

Dunbar, M. J., & Acreman, M. C. (2001). Applied hydro-ecological science for the twenty-first century. *Hydro-ecology: Linking Hydrology and Aquatic Ecology, International Association of Hydrological Sciences*, *266*, 1–17.

Durack, P. J., Wijffels, S. E., & Matear, R. J. (2012). Ocean salinities reveal strong global water cycle intensification during 1950 to 2000. *Science*, *336*(6080), 455–458.

Eagleson, P. S. (1978). Climate, soil, and vegetation: 1. Introduction to water balance dynamics. *Water Resources Research*, *14*(5), 705–712.

Eagleson, P. S. (1982). Ecological optimality in water-limited natural soil-vegetation systems: 1. Theory and hypothesis. *Water Resources Research*, *18*(2), 325–340.

Eklundh, L. (1998). Estimating relations between AVHRR NDVI and rainfall in East Africa at 10-day and monthly time scales. *International Journal of Remote Sensing*, *19*(3), 563–570.

Fan, Y., Li, H., & Miguez-Macho, G. (2013). Global patterns of groundwater table depth. *Science*, *339*(6122), 940–943.

Faramarzi, M., Abbaspour, K. C., Vaghefi, S. A., Farzaneh, M. R., Zehnder, A. J., Srinivasan, R., & Yang, H. (2013). Modeling impacts of climate change on freshwater availability in Africa. *Journal of Hydrology*, *480*, 85–101.

Federer, C. A. (1979). A soil-plant-atmosphere model for transpiration and availability of soil water. *Water Resources Research*, *15*(3), 555–562.

Fisher, J. B., & Andreadis, K. M. (2014). Drought: Roles of precipitation, evapotranspiration, and soil moisture. In Y. Wang (Ed.), *Encyclopedia of natural resources: Air* (pp. 1015–1017). New York: Taylor and Francis.

Fisher, J. B., Sikka, M., Sitch, S., Ciais, P., Poulter, B., Galbraith, D., ... Malhi, Y. (2013). African tropical rainforest net CO_2 fluxes in the 20th century. *Philosophical Transactions of the Royal Society B – Biological Sciences*, *368*(1625). http://dx.doi.org/10.1098/rstb.2012.0376.

Friedl, M. A., Sulla-Menashe, D., Tan, B., Schneider, A., Ramankutty, N., Sibley, A., & Huang, X. (2010). MODIS collection 5 global land cover: Algorithm refinements and characterization of new datasets. *Remote Sensing of Environment*, *114*(1), 168–182.

Grimm, N. B., Chapin, F. S., III, Bierwagen, B., Gonzalez, P., Groffman, P. M., Luo, Y., ... Williamson, C. E. (2013). The impacts of climate change on ecosystem structure and function. *Frontiers in Ecology and the Environment*, *11*(9), 474–482.

Guan, K., Wood, E. F., & Caylor, K. K. (2012). Multi-sensor derivation of regional vegetation fractional cover in Africa. *Remote Sensing of Environment*, *124*, 653–665.

Guan, K., Wood, E. F., Medvigy, D., Kimball, J., Pan, M., Caylor, K. K., ... Jones, M. O. (2014). Terrestrial hydrological controls on land surface phenology of African savannas and woodlands. *Journal of Geophysical Research: Biogeosciences*, *119*(8), 1652–1669.

Guillod, B. P., Orlowsky, B., Miralles, D. G., Teuling, A. J., & Seneviratne, S. I. (2015). Reconciling spatial and temporal soil moisture effects on afternoon rainfall. *Nature Communications*, *6*, 6443. http://dx.doi.org/10.1038/ncomms7443.

Gunderson, L. H. (2000). Ecological resilience–in theory and application. *Annual Review of Ecology and Systematics*, *31*, 425–439.

Haddeland, I., Heinke, J., Biemans, H., Eisner, S., Flörke, M., Hanasaki, N., ... Wisser, D. (2014). Global water resources affected by human interventions and climate change. *Proceedings of the National Academy of Sciences*, *111*(9), 3251–3256.

Harris, A., Carr, A. S., & Dash, J. (2014). Remote sensing of vegetation cover dynamics and resilience across southern Africa. *International Journal of Applied Earth Observation and Geoinformation*, *28*, 131–139.

Helm, K. P., Bindoff, N. L., & Church, J. A. (2010). Changes in the global hydrological-cycle inferred from ocean salinity. *Geophysical Research Letters*, *37*(18).

Holling, C. S. (1973). Resilience and stability of ecological systems. *Annual Review of Ecology and Systematics*, 1–23.

Huffman, G. J., Adler, R. F., Bolvin, D. T., Gu, G., Nelkin, E. J., Bowman, K. P., ... Wolff, D. B. (2007). The TRMM multi-satellite precipitation analysis: Quasi-global, multi-year, combined-sensor precipitation estimates at fine scale. *Journal of Hydrometeorology*, *8*(1), 38–55.

Hunt, E. R., Li, L., Yilmaz, M. T., & Jackson, T. J. (2011). Comparison of vegetation water contents derived from shortwave-infrared and passive-microwave sensors over central Iowa. *Remote Sensing of Environment*, *115*(9), 2376–2383.

Huntington, T. G. (2006). Evidence for intensification of the global water cycle: Review and synthesis. *Journal of Hydrology*, *319*(1), 83–95.

Ives, A. R., & Carpenter, S. R. (2007). Stability and diversity of ecosystems. *Science*, *317*(5834), 58–62.

Janowiak, J. E. (1988). An investigation of interannual rainfall variability in Africa. *Journal of Climate*, *1*(3), 240–255.

Jones, A. R., & Brunsell, N. A. (2009). A scaling analysis of soil moisture–precipitation interactions in a regional climate model. *Theoretical and Applied Climatology*, *98*(3–4), 221–235.

Jones, M. O., Jones, L. A., Kimball, J. S., & McDonald, K. C. (2011). Satellite passive microwave remote sensing for monitoring global land surface phenology. *Remote Sensing of Environment*, *115*(4), 1102–1114.

Jones, M. O., Kimball, J. S., Jones, L. A., & McDonald, K. C. (2012). Satellite passive microwave detection of North America start of season. *Remote Sensing of Environment*, *123*, 324–333.

Jones, M. O., Kimball, J. S., Small, E. E., & Larson, K. M. (2013). Comparing land surface phenology derived from satellite and GPS network microwave remote sensing. *International Journal of Biometeorology*, *58*(6), 1305–1315.

Kabanda, T. A., & Jury, M. R. (1999). Inter-annual variability of short rains over northern Tanzania. *Climate Research*, *13*(3), 231–241.

Khamis, G., & Papenbrock, J. (2014). Newly established drought-tolerant plants as renewable primary products as source of bioenergy. *Emirates Journal of Food and Agriculture*, *26*(12), 1067–1080. http://dx.doi.org/10.9755/ejfa.v26i12.19108.

Klaus, M., Holsten, A., Hostert, P., & Kropp, J. P. (2011). Integrated methodology to assess windthrow impacts on forest stands under climate change. *Forest Ecology and Management*, *261*(11), 1799–1810.

Konar, M., Jason Todd, M., Muneepeerakul, R., Rinaldo, A., & Rodriguez-Iturbe, I. (2013). Hydrology as a driver of biodiversity: Controls on carrying capacity, niche formation, and dispersal. *Advances in Water Resources*, *51*, 317–325.

Le Maitre, D. C., Scott, D. F., & Colvin, C. (1999). A review of information on interactions between vegetation and groundwater. *Water SA*, *25*, 137–152.

Li, L., Gaiser, P. W., Gao, B. C., Bevilacqua, R. M., Jackson, T. J., Njoku, E. G., ... Bindlish, R. (2010). WindSat global soil moisture retrieval and validation. *IEEE Transaction on Geoscience and Remote Sensing*, *48*(5), 2224–2241.

Liu, Y. Y., de Jeu, R. A., McCabe, M. F., Evans, J. P., & van Dijk, A. I. J. M. (2011). Global long-term passive microwave satellite-based retrievals of vegetation optical depth. *Geophysical Research Letters*, *38*, L18402. http://dx.doi.org/10.1029/2011GL048684.

Liu, Y., de Jeu, R. A., van Dijk, A. I. J. M., & Owe, M. (2007). TRMM-TMI satellite observed soil moisture and vegetation density (1998–2005) show strong connection with El Niño in eastern Australia. *Geophysical Research Letters*, *34*, L15401. http://dx.doi.org/10.1029/2007GL030311.

Liu, Y. Y., Evans, J. P., McCabe, M. F., de Jeu, R. A., van Dijk, A. I. J. M., Dolman, A. J., & Saizen, I. (2013). Changing climate and overgrazing are decimating Mongolian steppes. *PloS One*, *8*(2), e57599.

Liu, Z., Notaro, M., & Gallimore, R. (2010). Indirect vegetation–soil moisture feedback with application to Holocene North Africa climate. *Global Change Biology*, *16*(6), 1733–1743.

Liu, Y. Y., van Dijk, A. I. J. M., McCabe, M. F., Evans, J. P., & Jeu, R. A. (2012). Global vegetation biomass change (1988–2008) and attribution to environmental and human drivers. *Global Ecology and Biogeography*, *22*(6), 692–705.

Llopart, M., Coppola, E., Giorgi, F., da Rocha, R. P., & Cuadra, S. V. (2014). Climate change impact on precipitation for the Amazon and La Plata basins. *Climatic Change*, *125*(1), 111–125.

McCann, K. S. (2000). The diversity–stability debate. *Nature*, *405*(6783), 228–233.

McPherson, G. R. (1997). *Ecology and management of North American savannas.* University of Arizona Press.

McVicar, T. R., Roderick, M. L., Donohue, R. J., & Van Niel, T. G. (2012). Less bluster ahead? Ecohydrological implications of global trends of terrestrial near-surface wind speeds. *Ecohydrology*, *5*(4), 381–388.

Mladenova, I. E., Jackson, T. J., Njoku, E., Bindlish, R., Chan, S., Cosh, M. H., ... Santi, E. (2014). Remote monitoring of soil moisture using passive microwave-based techniques—Theoretical basis and overview of selected algorithms for AMSR-E. *Remote Sensing of Environment*, *144*, 197–213.

Morrongiello, J. R., Beatty, S. J., Bennett, J. C., Crook, D. A., Ikedife, D. N., Kennard, M. J., ... Rayner, T. (2011). Climate change and its implications for Australia's freshwater fish. *Marine and Freshwater Research*, *62*(9), 1082–1098.

Müller, C., Cramer, W., Hare, W. L., & Lotze-Campen, H. (2011). Climate change risks for African agriculture. *Proceedings of the National Academy of Sciences*, *108*(11), 4313–4315.

Müller, C., Waha, K., Bondeau, A., & Heinke, J. (2014). Hotspots of climate change impacts in sub-Saharan Africa and implications for adaptation and development. *Global Change Biology*, *20*(8), 2505–2517.

Nicholson, S. E. (1996). A review of climate dynamics and climate variability in eastern Africa. *The limnology, climatology and paleoclimatology of the East African lakes*, 25–56.

Nicholson, S. E. (2000). The nature of rainfall variability over Africa on time scales of decades to millenia. *Global and Planetary Change*, *26*(1), 137–158.

Nicholson, S. E., Davenport, M. L., & Malo, A. R. (1990). A comparison of the vegetation response to rainfall in the Sahel and East Africa, using normalized difference vegetation index from NOAA AVHRR. *Climatic Change*, *17*(2–3), 209–241.

Njoku, E. G., & Li, L. (1999). Retrieval of land surface parameters using passive microwave measurements at 6–18 GHz. *IEEE Transactions on Geoscience and Remote Sensing*, *37*(1), 79–93.

Njoku, E. G., Jackson, T. J., Lakshmi, V., Chan, T. K., & Nghiem, S. V. (2003). Soil moisture retrieval from AMSR-E. *IEEE Transaction on Geoscience and Remote Sensing*, *41*(2), 215–229.

Noy-Meir, I. (1973). Desert ecosystems: Environment and producers. *Annual Review of Ecology and Systematics*, 25–51.

O'Brien, K., Leichenko, R., Kelkar, U., Venema, H., Aandahl, G., Tompkins, H., ... West, J. (2004a). Mapping vulnerability to multiple stressors: Climate change and globalization in India. *Global Environmental Change*, *14*(4), 303–313.

O'Brien, K., Sygna, L., & Haugen, J. E. (2004b). Vulnerable or resilient? A multi-scale assessment of climate impacts and vulnerability in Norway. *Climatic Change*, *64*(1–2), 193–225.

Ogallo, L. J. (1988). Relationships between seasonal rainfall in East Africa and the southern oscillation. *Journal of Climatology*, *8*(1), 31–43.

Orellana, F., Verma, P., Loheide, S. P., & Daly, E. (2012). Monitoring and modeling water-vegetation interactions in groundwater-dependent ecosystems. *Reviews of Geophysics*, *50*(3).

Owe, M., De Jeu, R., & Holmes, T. (2008). Multisensor historical climatology of satellite-derived global land surface moisture. *Journal of Geophysical Research: Earth Surface (2003−2012)*, *113*(F1).

Owe, M., De Jeu, R., & Walker, J. (2001). A methodology for surface soil moisture and vegetation optical depth retrieval using the microwave polarization difference index. *IEEE Transactions on Geoscience and Remote Sensing*, *39*(8), 1643–1654.

Parinussa, R. M., Holmes, T. R., & De Jeu, R. A. (2012). Soil moisture retrievals from the WindSat spaceborne polarimetric microwave radiometer. *IEEE Transactions on Geoscience and Remote Sensing*, *50*(7), 2683–2694.

Pettorelli, N. (2013). *The normalized differential vegetation index*. Oxford, UK: Oxford University Press.

Pickett, S. T. (1985). *The ecology of natural disturbance and patch dynamics*. Academic press.

Pik, R. (2011). Geodynamics: East Africa on the rise. *Nature Geoscience*, *4*(10), 660–661.

Porporato, A., & Rodriguez-Iturbe, I. (2002). Ecohydrology-a challenging multidisciplinary research perspective/Ecohydrologie: Une perspective stimulante de recherche multidisciplinaire. *Hydrological Sciences Journal*, *47*(5), 811–821.

Richard, Y., & Poccard, I. (1998). A statistical study of NDVI sensitivity to seasonal and interannual rainfall variations in Southern Africa. *International Journal of Remote Sensing*, *19*(15), 2907–2920.

Robinson, D. A., Campbell, C. S., Hopmans, J. W., Hornbuckle, B. K., Jones, S. B., Knight, R., ... Wendroth, O. (2008). Soil moisture measurement for ecological and hydrological watershed-scale observatories: A review. *Vadose Zone Journal*, *7*(1), 358–389.

Rodhe, H., & Virji, H. (1976). Trends and periodicities in East African rainfall data. *Monthly Weather Review*, *104*(3), 307–315.

Rodriguez-Iturbe, I. (2000). Ecohydrology: A hydrologic perspective of climate-soil-vegetation dynamies. *Water Resources Research*, *36*(1), 3–9.

Römer, H., Willroth, P., Kaiser, G., Vafeidis, A. T., Ludwig, R., Sterr, H., & Revilla Diez, J. (2012). Potential of remote sensing techniques for tsunami hazard and vulnerability analysis–a case study from Phang-Nga province, Thailand. *Natural Hazards and Earth System Science*, *12*(6), 2103–2126.

Rossatto, D. R., Silva, L. D. C. R., Villalobos-Vega, R., Sternberg, L. D. S. L., & Franco, A. C. (2012). Depth of water uptake in woody plants relates to groundwater level and vegetation structure along a topographic gradient in a neotropical savanna. *Environmental and Experimental Botany*, *77*, 259–266.

Werner, P. A. (Ed.). (2009). *Savanna ecology and management: Australian perspectives and intercontinental comparisons*. John Wiley & Sons.

Schewe, J., Heinke, J., Gerten, D., Haddeland, I., Arnell, N. W., Clark, D. B., ... Kabat, P. (2014). Multimodel assessment of water scarcity under climate change. *Proceedings of the National Academy of Sciences*, *111*(9), 3245–3250.

Shi, J., Jackson, T., Tao, J., Du, J., Bindlish, R., Lu, L., & Chen, K. S. (2008). Microwave vegetation indices for short vegetation covers from satellite passive microwave sensor AMSR-E. *Remote Sensing of Environment*, *112*(12), 4285–4300.

Shinoda, M. (1995). Seasonal phase lag between rainfall and vegetation activity in tropical Africa as revealed by NOAA satellite data. *International Journal of Climatology*, *15*(6), 639–656.

Smith, A. M., Kolden, C. A., Tinkham, W. T., Talhelm, A. F., Marshall, J. D., Hudak, A. T., ... Gosz, J. R. (2014). Remote sensing the vulnerability of vegetation in natural terrestrial ecosystems. *Remote Sensing of Environment*, *154*, 322–337.

Sousa, W. P. (1984). The role of disturbance in natural communities. *Annual Review of Ecology and Systematics*, 353–391.

Stampoulis, D., Haddad, Z. S., & Anagnostou, E. N. (2014). Assessing the drivers of biodiversity in Madagascar by quantifying its hydrologic properties at the watershed scale. *Remote Sensing of Environment*, *148*, 1–15.

Tian, Y., & Peters-Lidard, C. D. (2010). A global map of uncertainties in satellite-based precipitation measurements. *Geophysical Research Letters*, *37*(24), L24407.

Traore, A. K., Ciais, P., Vuichard, N., MacBean, N., Dardel, C., Poulter, B., ... Myneni, R. (2014). 1982–2010 trends of light use efficiency and inherent water use efficiency in African vegetation: Sensitivity to climate and atmospheric CO_2 concentrations. *Remote Sensing*, *6*(9), 8923–8944.

Turk, J. F., Li, L., & Haddad, Z. S. (2014). A physically based soil moisture and microwave emissivity data set for global precipitation measurement (GPM) applications. *IEEE Transactions on Geoscience and Remote Sensing*, *52*(12), 7637–7650.

Turner, B. L., Kasperson, R. E., Matson, P. A., McCarthy, J. J., Corell, R. W., Christensen, L., ... Schiller, A. (2003). A framework for vulnerability analysis in sustainability science. *Proceedings of the National Academy of Sciences*, *100*(14), 8074–8079.

van Dijk, A. I. J. M., Beck, H. E., Crosbie, R. S., Jeu, R. A., Liu, Y. Y., Podger, G. M., ... Viney, N. R. (2013). The millennium drought in southeast Australia (2001–2009): Natural and human causes and implications for water resources, ecosystems, economy, and society. *Water Resources Research*, *49*(2), 1040–1057.

Verschuren, D., Laird, K. R., & Cumming, B. F. (2000). Rainfall and drought in equatorial east Africa during the past 1100 years. *Nature*, *403*(6768), 410–414.

Vinya, R., Malhi, Y., Brown, N., & Fisher, J. B. (2012). Functional coordination between branch hydraulic properties and leaf functional traits in miombo woodlands: Implications for water stress management and species habitat preference. *Acta Physiologiae Plantarum*, *34*(5), 1701–1710.

Vinya, R., Malhi, Y., Fisher, J. B., Brown, N., Brodribb, T., & Aragão, L. E. (2013). Xylem cavitation vulnerability influences tree species' habitat preference in miombo woodlands. *Oecologia*, *173*, 711–720.

Wolff, C., Haug, G. H., Timmermann, A., Damsté, J. S. S., Brauer, A., Sigman, D. M., ... Verschuren, D. (2011). Reduced interannual rainfall variability in East Africa during the last ice age. *Science*, *333*(6043), 743–747.